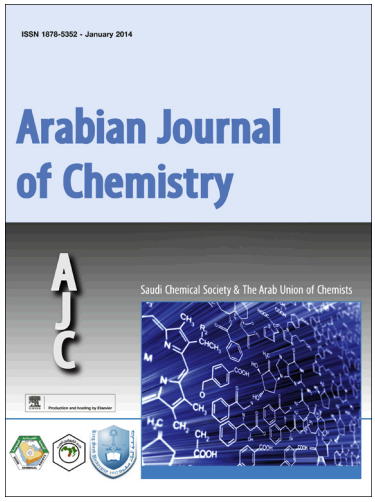

Original article

Synthesis, characterization and batch assessment of groundwater fluoride removal capacity of trimetal Mg/Ce/Mn oxide-modified diatomaceous earth

Wilson M. Gitari, Anthony A. Izuagie, Jabulani R. Gumbo

PII: S1878-5352(17)30005-9
DOI: http://dx.doi.org/10.1016/j.arabjc.2017.01.002
Reference: ARABJC 2040

To appear in: *Arabian Journal of Chemistry*

Received Date: 18 February 2016
Revised Date: 5 January 2017
Accepted Date: 6 January 2017

Please cite this article as: W.M. Gitari, A.A. Izuagie, J.R. Gumbo, Synthesis, characterization and batch assessment of groundwater fluoride removal capacity of trimetal Mg/Ce/Mn oxide-modified diatomaceous earth, *Arabian Journal of Chemistry* (2017), doi: http://dx.doi.org/10.1016/j.arabjc.2017.01.002

Synthesis, characterization and batch assessment of groundwater fluoride removal capacity of trimetal Mg/Ce/Mn oxide-modified diatomaceous earth

Wilson M. Gitari[1,a], Anthony A. Izuagie[1,a,*], Jabulani R. Gumbo [2,a]

[1]Department of Ecology and Resource Management, University of Venda, Thohoyandou, South Africa; E-mails: mugera.gitari@univen.ac.za; aaizuagie@gmail.com;.

[2]Department of Hydrology and Water Resources, University of Venda, Thohoyandou, South Africa; E-mail: Jabulani.gumbo@univen.ac.za.

[a]Environmental Remediation and Pollution Chemistry Research Group, School of Environmental Sciences, University of Venda, Thohoyandou, South Africa.

*Corresponding author: E-mail: aaizuagie@gmail.com; Tel.: +27 717 228 420.

Abstract In this study, trimetal Mg/Ce/Mn oxide-modified diatomaceous earth (DE) was synthesized at optimal conditions. Comparison of the SEM images and the results of EDX analyses of the raw and the modified DE confirmed the surface modification of the raw DE with the trimetal oxide. Groundwater fluoride removal capacity of the sorbent was evaluated by batch method at various defluoridation conditions. At a sorbent dosage of 0.6 g/100 mL (contact time: 60 min, mixing speed of 200 rpm and temperature: 297 K), the fluoride removal was > 93% for solutions containing initial fluoride concentration of 10 mg/L - 60 mg/L. Sorbent's optimum fluoride uptake capacity was 12.63 mg/g at the initial fluoride concentration of 100 mg/L. Fluoride removal was > 91% for solutions with initial pH range of ~ 4 to 11 (initial fluoride concentration: 9 mg/L, sorbent dosage: 0.6 g/100 mL). Appraisal of the effect of co-existing anions on fluoride removal showed that CO_3^{2-} would reduce the amount of fluoride removed from solution, while other anions such as PO_4^{3-}, NO_3^- and SO_4^{2-} had no observable effect. K_2SO_4 solution was found to be most suitable for regeneration of spent Mg/Ce/Mn oxide-modified DE compared to Na_2CO_3 and NaOH. The mechanism of fluoride removal at pH > 5.45 (pHpzc = 5.45) occurred by exchange of hydroxyl groups on surface of sorbent with fluoride ions from solution. Sorption data fitted better to Langmuir isotherm and pseudo-second-order model. External diffusion was observed to be the sorption rate limiting factor.

Keywords: synthesis; trimetal oxide-modified diatomaceous earth; defluoridation, groundwater

1. Introduction

Human need for clean water cannot be overemphasized. The total body water of an average young adult male for example is 50 to 70% of the body weight (Altman, 1961). Potable water is however scarce since clean water does not occur in nature (Gambhir et al., 2012). Water from natural sources contains different dissolved salts apart from suspended particles. Primarily, the salts and minerals in surface and groundwater originate from the soil and rock with which it is in contact.

In developing countries, including South Africa, the right drinking-water for rural communities where there is no pipe-borne water is groundwater (Ncube and Schutte, 2005). Most of the surface waters in the rural communities are susceptible to pollution by human and animal faeces (Obi et al., 2002), thereby exposing direct consumers to health risk. Therefore, reliance on groundwater as alternative drinking-water becomes germane.

Though the consumption of groundwater reduced cases of water-borne diseases, there are new problems arising from its consumption (Daw, 2004). Fluoride is important for the development of healthy teeth if it is present in groundwater (drinking-water) at appropriate concentrations. But if drinking-water contains fluoride at concentrations above the World Health Organization (WHO) guideline of 1.5 mg/L (WHO, 2011), diseases known as dental and skeletal fluorosis could arise. The severity of either fluorosis is much dependent on the concentration of fluoride and the period of exposure (Jenkins, 1978; Teri, 1982; Abdulrahmani, 1996). It is important to reduce the fluoride in drinking water to an acceptable level for drinking. The techniques that have been employed for this purpose include adsorption, ion-exchange, precipitation/coagulation, and membrane processes (Hichour et al., 2000; Amor et al., 2001). Adsorption technique has gained more prominence over other techniques majorly because of its simplicity and low cost (Mjengera and Mkongo, 2003).

Diatomaceous earth (DE) has found variety of uses industrially because of some of its advantageous physical and chemical properties which include high porosity (80-90% void), large surface area, high liquid absorption capacity, low thermal conductivity and chemical inertness (Lemonas, 1997; Antonides, 1998). The use of DE in adsorption technology for water treatment received much consideration in recent times essentially because of its high porosity which is an advantage for metal oxide infusion for metal and non-metal removal from water and industrial effluents (Khraisheh et al., 2004a, 2004b; Oladoja and Helmreich, 2014).

Binary metal Al/Fe oxide-modified DE was earlier reported by Izuagie et al. (2016) to be a more effective sorbent than either Al or Fe oxide-modified DE for groundwater defluoridation. The synergy of the two metals in Al/Fe oxide-modified DE towards increase in fluoride removal was a motivation for the synthesis and appraisal of defluoridation capacity of a trimetal oxide-modified DE with a specific interest in the oxides of magnesium (Mg), cerium (Ce) and manganese (Mn) in the sorbent composite. It was important to evaluate whether the number of metals in a sorbent was a consistent determinant of enhanced fluoride adsorption.

The fluoride removal effectiveness of Mg, Ce or Mn oxides individually or in combination with other metal oxides from water has been widely reported (Wu et al., 2007; Wang et al., 2015). Therefore, in this study, there was optimized synthesis of Mg/Ce/Mn trimetal oxide-modified DE, characterization and evaluation of the fluoride uptake capacity of the sorbent at optimized conditions.

2. Materials and methods

2.1. Sample preparation

Some diatomaceous earth (DE) obtained from natural deposits at Kariandusi in Gilgil District, Nakuru County, Kenya was crushed in the mortar and dispersed in a large amount of Milli-Q water (18.2 MΩ cm @ 25 ^{0}C) in a liter glass beaker. The suspension was stirred for some time to release trapped sand and silt from the DE. Floating debris and dirt were removed from the surface of suspension with spatula while the basal sand and silt were removed through repeated process of water addition and decantation of suspension. The sand and silt-free suspension was centrifuged to discard the supernatant.

The clean DE was then scooped into some fresh Milli-Q water in a liter flask, stirred and the pH adjusted to 11 using 0.1 M NaOH solution. The bottle was corked and shaken on Stuart reciprocating shaker at 200 rpm for 30 min. After equilibration, the mixture was centrifuged at 5000 rpm to recover the solid to remove the supernatant. The NaOH-treated DE was acidified with 0.1 M HCl to pH 2 and also shaken in a corked liter flask at 200 rpm for 30 min. After equilibration, the mixture was centrifuged and the solid washed with a large volume of Milli-Q water. The washed solid was dried in the oven at 110 ^{0}C for 8 h, cooled in the desiccator and then stored in corked plastic bottles for subsequent use.

2.2. Solution preparation

The salt solutions for DE modification as well as different fluoride solutions were prepared from analytical grade chemicals which included sodium fluoride (NaF), magnesium tetraoxosulphate (VI) ($MgSO_4$), cerium (III) chloride heptahydrate ($CeCl_3.7H_2O$) and manganese (II) chloride tetrahydrate ($MnCl_2.4H_2O$). All the chemicals were supplied by Rochelle Chemicals, South Africa.

For the optimized modification of diatomaceous earth with Mg/Ce/Mn oxide, 50 mL of 0.25 M $MgSO_4$, 50 mL of 0.25 M $CeCl_3.7H_2O$ and 100 mL of 0.25 M $MnCl_2.4H_2O$ solutions were prepared by dissolving 1.5046 g, 4.6573 g and 4.9478 g of the respective salts in Milli-Q water in appropriate volumetric flasks and then raising the volume to the etched mark by adding more Milli-Q water. The flasks were stoppered and shaken to attain homogeneity.

2.3. Synthesis and optimization of Mg/Ce/Mn oxide-modified diatomaceous earth

It was important to first evaluate the defluoridation potentials of Ce oxide-modified DE (Ce-DE) and Mn oxide-modified DE (Mn-DE) in order to estimate the contribution of each metal oxide to the overall defluoridation properties of the binary Ce/Mn oxide-modified DE (Ce-Mn-DE). To achieve this aim, one gram each of DE was weighed into 15 mL of 0.25 M Ce^{3+} and 15 mL of 0.25 M Mn^{2+} in separate 250 mL plastic bottles. The mixtures were swirled for about 1 min and shaken at 100 rpm on a reciprocating shaker for 20 min to soak. The pH of each mixture was adjusted to 8.25 with the addition of 2 M NaOH to precipitate the metal hydroxides. The bottles were corked and shaken at 100 rpm for 30 min. The mixture containing Ce was centrifuged after 1 h while the one containing Mn was left exposed to air for 10 h for oxidation of Mn^{2+} to Mn^{4+} before centrifuging. Each mixture was washed with 100 mL of Milli-Q water, centrifuged, the solid dried at 110 ^{0}C for 8 h and then cooled in a desiccator.

Ce-Mn-DE was obtained by modifying also 1 g of DE with combined 7.5 mL of 0.25 M Ce^{3+} and 7.5 mL of 0.25 M Mn^{2+} following the same procedure as Ce-DE and Mn-DE modifications.

A mass of 0.4 g of each modified species was contacted with 50 mL of 10 mg/L fluoride solution at 200 rpm for 30 min. The equilibrium pH of each mixture was measured to evaluate the pH status of treated water. While the equilibrium pH of treated water was circum-neutral with the use of Mn-DE, the water treated with Ce-DE was acidic (Table 1). After the equilibrium pH measurement, the mixtures were centrifuged and the supernatants analyzed for residual fluoride.

Addition of $Mg(OH)_2$ to the composite of Ce and Mn oxide-modified DE was contemplated to increase the pH of treated water to circum-neutral level. It was therefore necessary to add the solutions of the three metal salts together at different proportions in order to evaluate a modified product which would not only have a very high fluoride removal capability but also yield treated water with circum-neutral pH. The three salt solutions prepared for the modification of DE (subsection 2.2) were added together in a 250 mL plastic bottle at different proportions. The total volume of each solution mixture was 20 mL (Table 2).

A mass of 3 g of DE was weighed into each solution and shaken for 20 min at 100 rpm, for proper soaking. The pH of the suspensions was adjusted to 8.2 by adding 2 M NaOH with vigorous mixing. After the pH adjustment, the bottles were corked and the suspensions shaken on a Stuart reciprocating shaker at 150 rpm for 30 min. Each content was then exposed to air for 10 h for possible oxidation of Mn^{2+} to Mn^{4+}. The modified DE was separated from the mixture by centrifuging. Each solid was then washed with 100 mL of Milli-Q water followed by centrifuging to remove the supernatant. The clean solids were dried in the oven at 110 ^{0}C for 8 h and then cooled in a desiccator. The samples were crushed in the mortar, passed through 250 μm test sieve and finally stored in corked plastic bottles to prevent moisture.

2.4. Batch defluoridation with Mg/Ce/Mn oxide-modified diatomaceous earth

The performance of Mg/Ce/Mn oxide-modified DE in fluoride removal from water was evaluated by batch adsorption method. Known masses of sorbent were weighed into 100 mL of fluoride concentrations in 250 mL plastic bottles. The bottles were corked and shaken inside Daihan LabTech Model LSB-015S reciprocating shaker at 200 rpm for 60 min or at different times where evaluation of effect of contact time was necessary. After equilibration, the mixtures were centrifuged at 5000 rpm for 5 min. Total Ionic Strength Adjustment Buffer III (TISAB III) was added to the supernatants and fluoride standards at volume ratio 1:10 and mixed thoroughly. The TISAB III-added supernatants stood for 40 min before fluoride analysis using four-standard calibrated ORION VERSASTAR Advanced Electrochemistry meter fluoride ion-selective electrode. TISAB III served to decomplex the metal-fluoride complex, maintain a constant ionic strength and adjust the pH to around 5.3 to prevent formation of HF or HF_2^- which cannot penetrate the electrode's membrane for measurement.

2.5. Pertinent computational equations

The percent fluoride removal was computed from the sorption data using Equation (1) given as:

$$\%\ F^{-}\ \text{removal} = \frac{(C_0 - C_e)}{C_0} \times 100 \quad (1)$$

C_0 (mg/L) and C_e (mg/L) are the initial and equilibrium fluoride concentrations respectively.

The adsorption capacity, q_e (mg/g) was computed using Equation (2):

$$\text{Adsorption capacity} = \frac{(C_0 - C_e)}{m} \times V \quad (2)$$

m (g) is the mass of adsorbent while V (L) is the volume of fluoride solution.

2.6. Scanning electron microscopy-energy dispersion X-ray (SEM-EDX) analysis

For the purpose of evaluating the extent of change at the DE's surface after the trimetal oxide coating, the trimetal oxide, the raw and the modified DE were scanned at the National Centre for Nano-Structured materials, Council for Scientific and Industrial Research (CSIR), South Africa using JEOL - JSM 7500F Scanning Electron Microscope. The elemental analysis was done using energy dispersion X-ray (EDX).

2.7. Surface area and pore volume analyses`

The surface area, pore area and pore volume of the trimetal oxide-modified DE were analyzed at the National Centre for Nano-Structured materials, Council for Scientific and Industrial Research (CSIR), South Africa, using a combined Brunauer–Emmett–Teller (BET) and Barrett-Joyner-Halenda (BJH) methods. The instrument for analysis was Micromeritics TriStar II *Surface Area and porosity*.

2.8. X-ray diffraction analysis

The X-ray diffraction analysis of the trimetal oxide-modified DE was carried out at the XRD & XRF Facility, Faculty of Natural & Agricultural Sciences, Department of Geology, University of Pretoria, South Africa using PANalytical X'Pert Pro powder diffractometer with X'Celerator detector and variable divergence- and fixed receiving slits with Fe filtered Co-Kα radiation. The phases were identified using X'Pert Highscore plus software.

2.9. Fourier Transform Infra-Red (FTIR) Spectroscopy

The FTIR spectroscopic analyses of Mg/Ce/Mn oxide, Mg/Ce/Mn oxide-modified DE and fluoride-loaded modified DE were run to identify the functional groups in the materials as

well as evaluate likely changes in the functional groups of the modified sorbent on contact with fluoride solution. The spectra of the trimetal oxide-modified and the fluoride-loaded form are characteristically different from that of the pure Mg/Ce/Mn oxide. For the two, the fingerprints of the silica bands are distinct. It could therefore be readily observed from the spectrum of Mg/Ce/Mn oxide that the material has no silica component.

2.10. Major and trace elements analyses

The X-ray fluorescence (XRF) analysis of the major elements in Mg/Ce/Mn oxide-modified DE was carried out at the ICP-MS and XRF Laboratory, Central Analytical Facilities, Stellenbosch University, South Africa, using PANalytical equipped with Rh tube. The full suit trace elements analysis was carried out using laser ablation ICP-MS on fusion disk.

2.11. Optimization of adsorption conditions

The effect of contact time on fluoride removal was evaluated using three adsorbent dosages (0.1 g, 0.2 g and 0.3 g). A mass of 0.1 g of adsorbent was weighed into aliquots of 100 mL of 10 mg/L fluoride solution in 250 mL plastic bottles at 297 K and agitated for 2, 5, 10, 20, 30, 40, 50, 60 and 70 min at a shaking rate of 200 rpm. The mixtures were then centrifuged with the supernatants analyzed for fluoride following the procedure explained in subsection 2.4. The experiment was repeated using sorbent dosages of 0.2 g and 0.3 g.

The effect of sorbent dosage on fluoride sorption was evaluated at 297 K using different masses of the adsorbent (0.1, 0.2, 0.3, 0.4, 0.6, 0.8 and 1 g) agitated in aliquots of 100 mL of 10 mg/L fluoride solution.

Evaluation of the effect of initial fluoride concentration on the extent of fluoride sorption onto the trimetal oxide-modified DE was evaluated at temperatures 297 K, 310 K and 326 K. At each temperature, 0.6 g each of sorbent was contacted with 10, 20, 30, 40, 50, 60, 80 and 100 mg/L fluoride in 250 mL plastic bottles for 60 min.

Fluoride sorption is broadly reported to be highly dependent on the pH of solution (Tripathy et al., 2006; Yadav et al., 2006; Kamble et al., 2009). Therefore, the effect of solution pH on fluoride sorption on Mg/Ce/Mn oxide-modifide DE was evaluated at initial pH 2 to 12 using 0.6 g/100 mL of sorbent while the initial fluoride concentration was 9 mg/L.

The effect of temperature on fluoride sorption onto Mg/Ce/Mn oxide-modified DE was evaluated at 297 K, 310 K and 326 K following the procedure for evaluating the effect of initial fluoride concentration. The choice of temperatures took into account the fact that at

least ten-degree rise in temperature, ordinarily, would cause the rate constant to double or triple in homogeneous thermal reactions (Upadhyay, 2006).

2.12. Effect of co-existing anions

Commonly, fluoride is not the only anion in groundwater. During defluoridation of groundwater using adsorption technique, anions other than fluoride could possibly interfere in the defluoridation process. NO_3^-, CO_3^{2-}, SO_4^{2-} and PO_4^{3-} are reported to have an effect on fluoride removal (Chen et al., 2011). The effect of each of the anions on fluoride removal was studied separately.

Simulated groundwater was prepared by measuring 1 mL of 1000 mg/L fluoride and 50 mL of 10 mg/L of the anion being evaluated into 100 mL volumetric flask. Milli-Q water was then added to the flask until the volume of solution was at the etched mark. The resultant solution which contained 10 mg/L fluoride and 5 mg/L anion was shaken thoroughly and then transferred into a 250 mL plastic bottle. In each determination, a mass of 0.6 g of adsorbent was contacted with 100 mL of "groundwater" for 60 min. The supernatants obtained after centrifuging were analyzed for fluoride as described in subsection 2.3.

2.13. Sorbent regeneration and reuse

Desorption study was carried out to evaluate the reusability of the spent sorbent. The solutions used for sorbent regeneration included 0.01 M NaOH and 0.1 M K_2SO_4 solutions. In each case, the first process involved defluoridation of 100 mL of 10 mg/L fluoride solution using 0.8 g of Mg/Ce/Mn oxide-modified DE. The mixtures were centrifuged and the supernatants analyzed for residual fluoride according to subsection 2.3. The separated solid was washed with Milli-Q water, dried in the oven at 110 ^{0}C for 8 h and then cooled in the desiccator. The dry solid was crushed and sieved with a 250 µm test sieve. The sieved, spent sorbent was weighed and equilibrated with 100 mL of each of the regenerants for 60 min to desorb fluoride. The process of centrifuging, washing of solid, desorbed fluoride measurement and drying of solids was as done in other defluoridation experiments. A known mass of dry, crushed and sieved sorbent was again contacted with 100 mL of 10 mg/L fluoride solution.

The regeneration of spent sorbent and defluoridation with the regenerated sorbent continued until the third cycle of defluoridation.

2.14. pH at Point-of-zero-charge (pHpzc)

The pH at point-of-zero charge of Mg/Ce/Mn oxide-modified DE was evaluated in 1 M, 0.1 M and 0.01 M KCl solutions in order to ascertain the consistency of result. The pH of solutions was adjusted to desired values by adding 0.1 M HCl or 0.1 M NaOH. The new pH therefore constituted the initial pH (pH_0) of solutions. Aliquots of 25 mL of solutions were pipetted into 50 mL plastic bottles. A mass of 0.2 g of adsorbent was then weighed into each of the bottles. The bottles were corked and shaken inside a thermostated water bath shaker at 200 rpm for 24 h. After equilibration, the equilibrium pH (pH_e) of each mixture was quickly measured and recorded.

3. Results and discussion

3.1. Synthesis and optimization of Mg/Ce/Mn oxide-modified diatomaceous earth

The results of fluoride analysis defluoridation using Ce-DE, Mn-DE and Ce-Mn-DE as discussed in subsection 2.3 are presented in Table 1. Table 1 shows that the percent fluoride removal by Ce-DE was more than eight times higher than that recorded for Mn-DE.

The synthesis of Ce-Mn-DE required half of the volume of Ce^{3+} solution used in the synthesis of Ce-DE, thereby making the synthesis of the former to have a better cost advantage in addition to removing more fluoride from solution.

Table 1 Fluoride removal by different samples of metal oxide-modified diatomaceous earth

Adsorbent	pH_0	pH_e	C_e (mg/L)	% F^- removal
Ce-DE	3.46	3.42	0.787	92.1
Mn-DE	6.50	7.07	8.940	10.6
Ce-Mn-DE	4.36	4.22	0.333	96.7

3.2. Modification and evaluation of defluoridation efficiencies of trimetal oxide-modified DE samples

Table 2 presents the various volumes of each modification solution added together to obtain a total solution mixture of 20 mL used to modify DE. The mixture ratios of Mg:Ce:Mn were consequently 1:1:6, 1:2:5, 2:1:5, 1:1:2, 4:1:3 and 2:1:1 respectively from the top down Table 2.

Table 2 Volumes of solutions of metal salts in mixtures

Volume of solution (mL)			Total volume (mL)
Mg^{2+}	Ce^{3+}	Mn^{2+}	
2.5	2.5	15	20
2.5	5.0	12.5	20
5.0	2.5	12.5	20
5.0	5.0	10.0	20
10	2.5	7.5	20
10	5.0	5.0	20

The results of the fluoride removal by each trimetal oxide-modified sample are reported in Table 3.

Comparatively, the highest fluoride removal of 71.2% occurred with the use of sorbent from reagents mixture ratio 2:1:1. However, to enhance fluoride removal for the sorbent with reagents mixture ratio 2:1:1, the concentration of each reagent was increased to 0.5 M. Thus, the percent fluoride removal with increase in reagents' concentrations was 94.7%. This shows that DE has the capacity for higher concentrations of metal oxides.

Table 3 Fluoride removal by trimetal oxide-modified diatomaceous earth samples

Trimetal oxide-modified DE from volume ratio (Mg:Ce:Mn)	pH_0	pH_e	C_e (mg/L)	% F^- removal
1:1:6	6.85	6.94	9.14	8.6
2:1:5	6.91	6.88	8.52	14.8
1:1:2	6.45	6.31	5.03	49.7
1:2:5	6.49	6.43	6.50	35.0
2:1:1	6.32	6.19	2.88	71.2
2:1:1*	6.36	6.19	0.53	94.7
4:1:3	6.82	6.74	7.66	23.4

*Diatomaceous earth modified with 0.5 M $MgSO_4$, 0.5 M $CeCl_3.7H_2O$ and 0.5 M $MnCl_2.4H_2O$.

The further reduction in the volume of Ce^{3+} required for the optimum synthesis of Mg/Ce/Mn oxide-modified DE made the sorbent synthesis most cost effective compared to Ce-DE and Ce-Mn DE.

3.3. Characterization of Mg/Ce/Mn oxide-modified diatomaceous earth

3.3.1. Scanning electron microscopy-energy dispersion X-ray (SEM-EDX) analysis

The images of the surface morphological structures of the raw DE, trimetal oxide and the modified DE are presented in Figure 1. With the coating of the raw DE with the trimetal oxide, the pores are less conspicuous (images e. and f.) than they were before modification was carried out (images a. and b.). Images c. and d. show the morphology of the Mg/Ce/Mn oxide.

The elemental analysis by energy dispersion X-ray (EDX) shows increase in the average number of atoms of the modification metals over the values in the raw sample (Figure 2). This is a further proof of modification of DE.

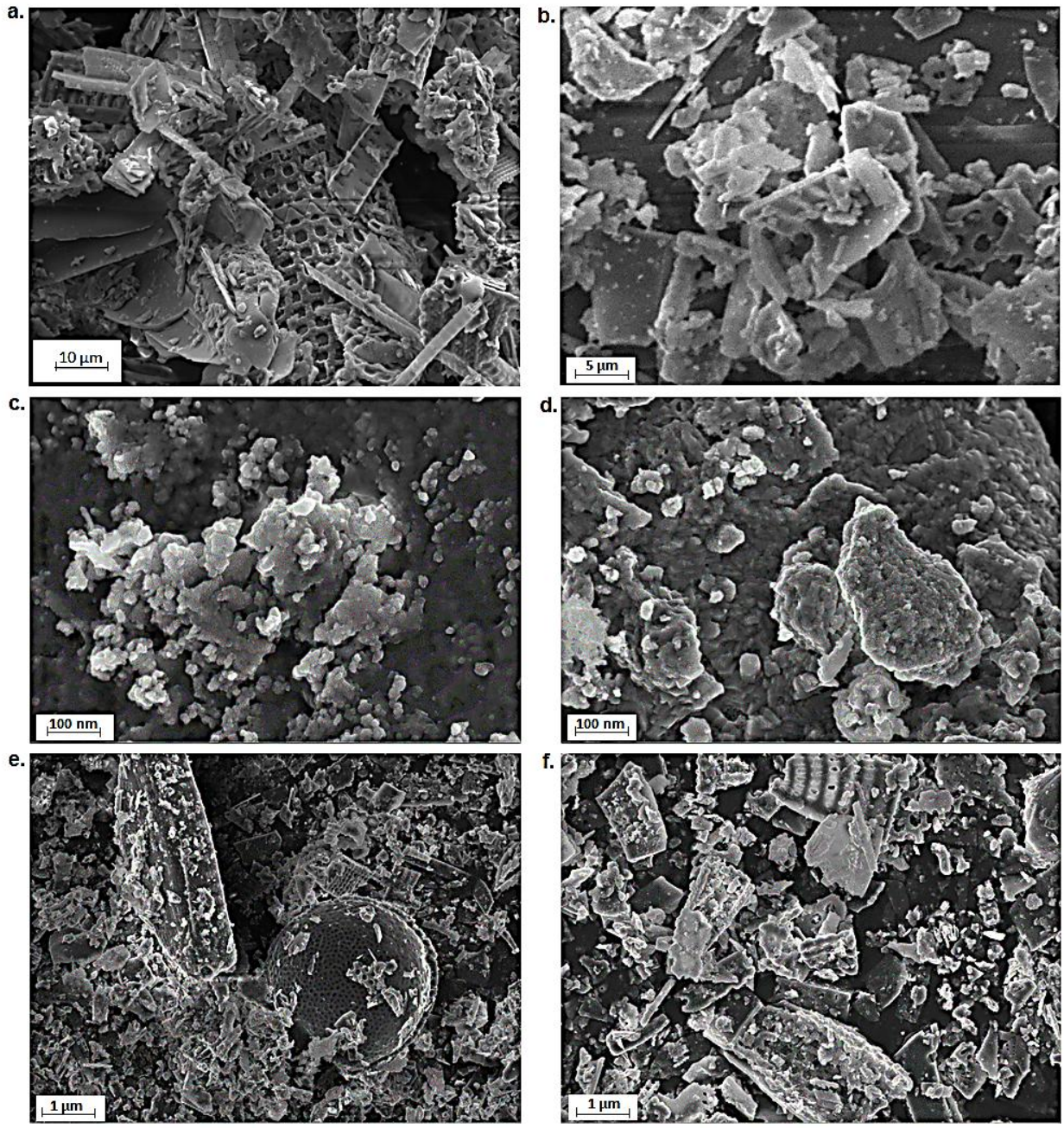

Figure 1 SEM images of raw diatomaceous earth (**a** & **b**), Mg/Ce/Mn oxide (**c** & **d**) and Mg/Ce/Mn oxide-modified diatomaceous earth (**e** & **f**).

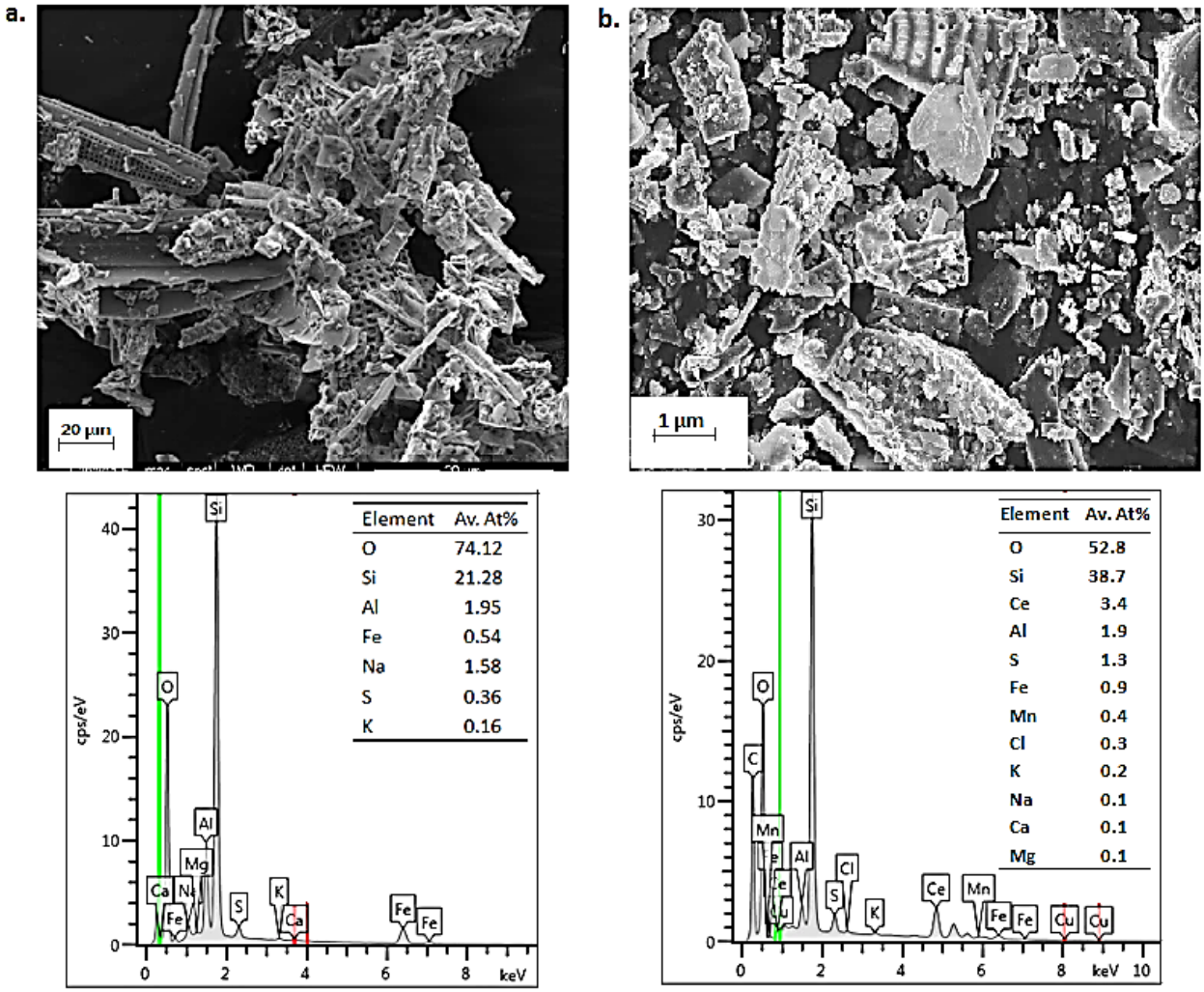

Figure 2 SEM image and EDX of **a.** raw diatomaceous earth, **b.** Mg/Ce/Mn oxide-modified diatomaceous earth.

3.3.2. Surface area and pore volume analyses

The BET surface area increased from 31.8861 ± 0.1619 m^2/g (for the raw DE) to 35.9056 ± 0.0816 m^2/g (for the modified sorbent). The deposit of Mg/Ce/Mn oxide on raw DE increased the surface area of DE. Thus, there were more active sorption sites on the trimetal oxide-modified DE with modification in line with the results reported in literature (Khraisheh et al., 2004b; Xiong and Peng, 2008; Datsko et al., 2011). The pore diameter of the bulk of the pores lied within the mesopores range of 2 nm – 50 nm as presented in Figure 3.

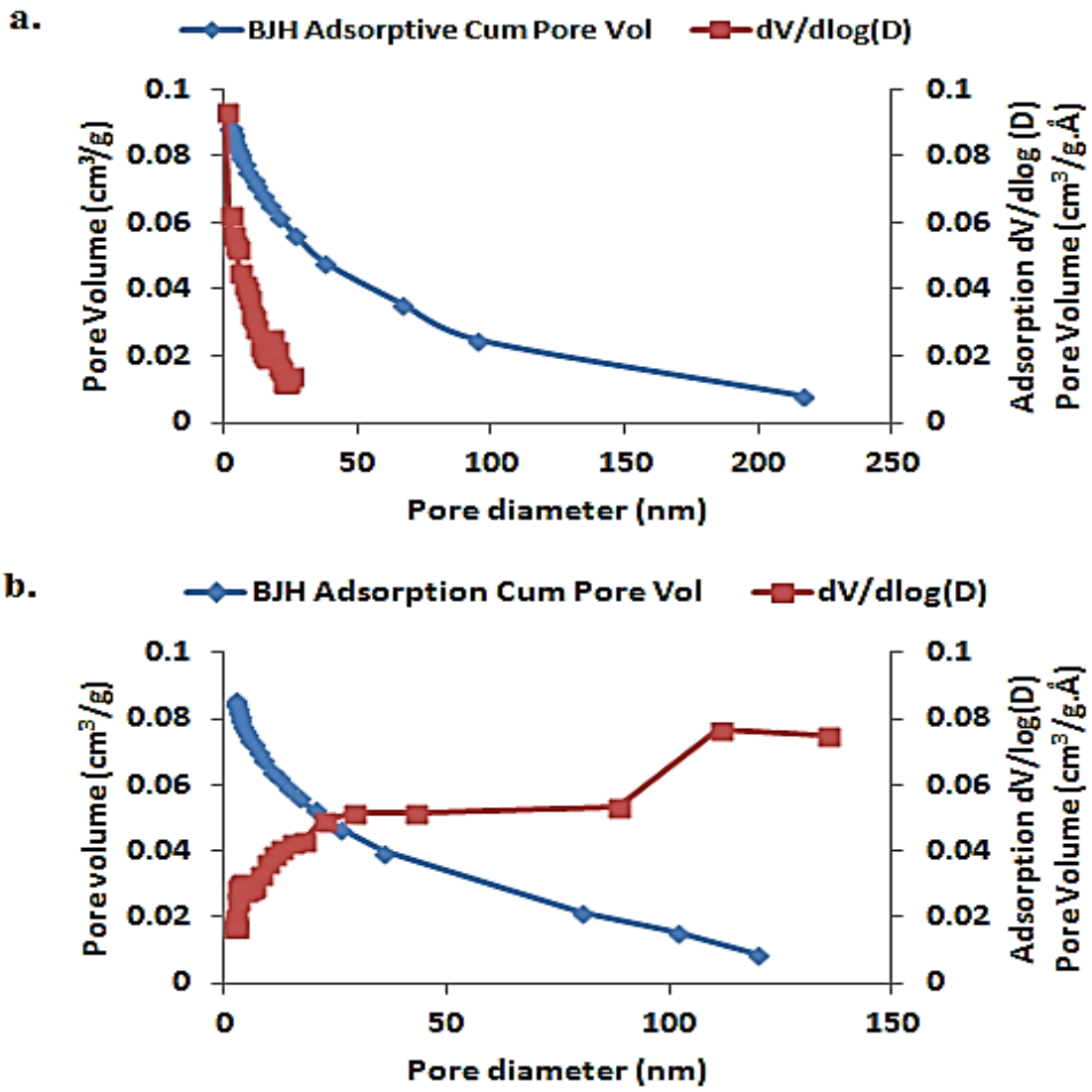

Figure 3 Plot of BJH adsorption pore volume and BJH dV/dlog(D) pore volume against pore diameter (D) for **a.** raw and **b.** Mg/Ce/Mn oxide-modified diatomaceous earth.

3.3.3. X-ray diffraction analysis

The X-ray diffractogram (Figure 4) of Mg/Ce/Mn oxide-modified DE shows that the material is completely amorphous as no peaks were visible which, are characteristics of crystalline materials. Hence, the modified DE had no crystalline mineral phase. The amorphous nature of the sorbent is an added advantage to its suitability for defluoridation.

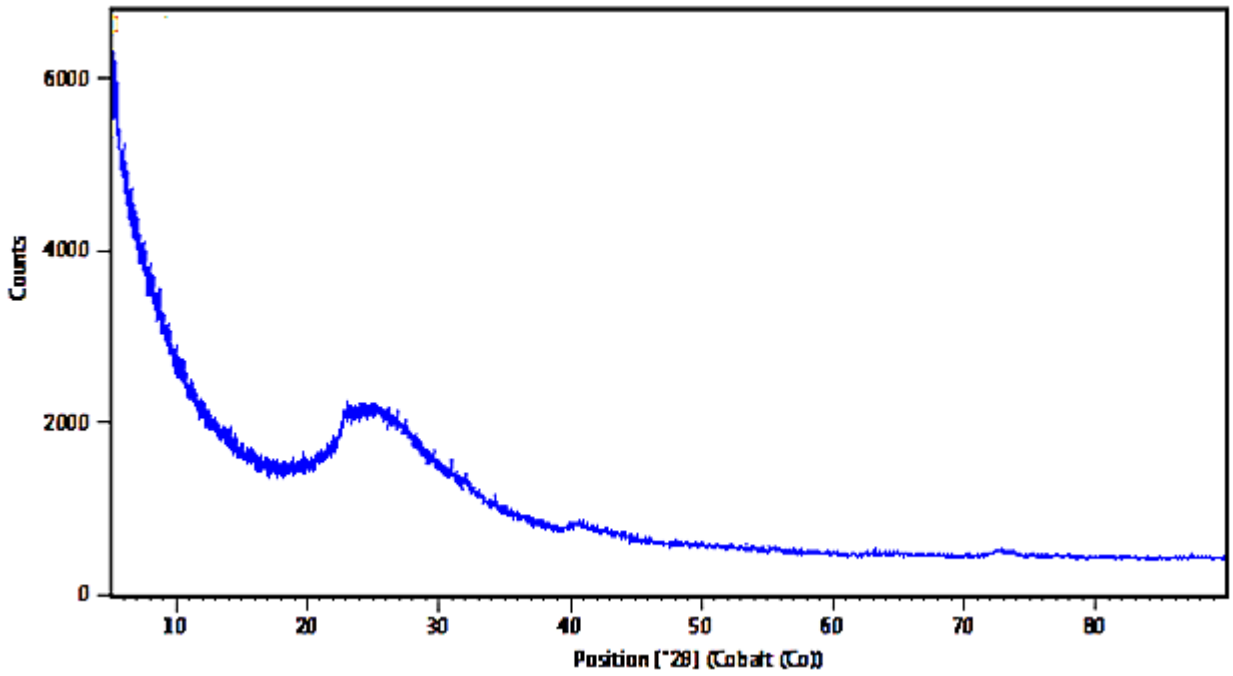

Figure 4 X-ray diffractogram of Mg/Ce/Mn oxide-modified diatomaceous earth.

3.3.4. Major and trace elements analyses

The results of the major elements reported in terms of the oxides of the elements were compared with those of the raw DE (Table 4). The percent compositions of the oxides of Mg and Mn in the modified species were observed to increase for the modified sample. The increase was most probably due to the use of the metal oxides in the modification of DE. There was however a notable decrease in the percent composition of SiO_2 from 84.17 to 69.41% with DE modification. The decrease was as a result of the large concentration of Ce oxide coating of DE revealed by the ICP-MS trace metal analysis of the sorbent (Table 5).

Table 5 shows a remarkable increase of Ce in the modified sorbent from 109.58 mg/kg (in the raw DE) to 89959.80 mg/kg (in the modified DE), accounting for ~ 9% of the sorbent mass. In other words, the value, 89959.80 mg/kg implies that 100 g of sorbent contained ~ 9 g of Ce. Comparing the percentage compositions of Mg, Ce and Mn in the sorbent, it is evident that Ce oxide constituted the major oxide in the sorbent and so would to a large extent influence the defluoridation characteristics of the sorbent.

Table 4 Comparison of the major elements in the raw and Mg/Ce/Mn oxide-modified diatomaceous earth

Oxide	% composition	
	Raw DE	Mg/Ce/Mn oxide-modified DE
SiO_2	84.17	69.41
Al_2O_3	4.01	3.10
Fe_2O_3	2.96	1.87
Na_2O	0.61	0.37
K_2O	0.75	0.39
MgO	0.11	0.27
CaO	0.24	0.13
ZrO_2	0.06	-
TiO_2	0.17	0.12
MnO	0.04	0.55
P_2O_5	0.04	0.03
*L.O.I.	7.52	4.99

***Loss on ignition**

Table 5 Comparison of concentration of trace metals in raw and Mg/Ce/Mn oxide-modified diatomaceous earth

Trace element	Concentration of trace elements (mg/kg)	
	Raw DE	Mg/Ce/Mn oxide modified DE
Sc	3.85	8.77
V	25.20	14.91
Cr	11.84	24.23
Co	1.43	1.21
Ni	7.38	14.33
Cu	17.55	16.59
Zn	86.93	70.91
Rb	44.67	30.15
Sr	26.74	10.06
Y	51.45	40.93
Zr	453.15	419.41
Nb	85.41	63.30
Mo	2.36	2.12
Cs	1.20	0.93
Ba	30.97	20.27
La	58.50	52.98
Ce	109.58	89 959.80
Pr	13.00	19.18
Nd	49.75	35.89
Sm	9.65	9.13
Eu	0.90	1.08
Gd	8.42	341.36
Tb	1.48	7.86
Dy	9.41	7.20
Ho	2.05	1.55
Er	6.13	4.78
Tm	0.91	0.66
Yb	6.24	4.68
Lu	0.89	0.71
Hf	11.32	10.08
Ta	5.04	3.81
Pb	11.08	7.76
Th	13.70	10.44
U	2.95	2.05

3.3.5. Fourier Transform Infra-Red (FTIR) Spectroscopy

Figure 5 shows that there was an increase in the transmittance of the band at the wavenumber 454 cm^{-1} for the modified DE. The band at 454 cm^{-1} represents the Si-O-H stretching

vibration, while the one at 1052 cm^{-1} represents the Si-O-Si stretching vibration. With some of the OH groups replaced by fluoride ions, there was a decrease in the number of Si-O-H groups. Therefore, there was a decrease in the absorbance of IR by the remaining Si-O-H groups. The bands around 3300 cm^{-1} for the three samples are for the -OH group from the adsorbed water molecules.

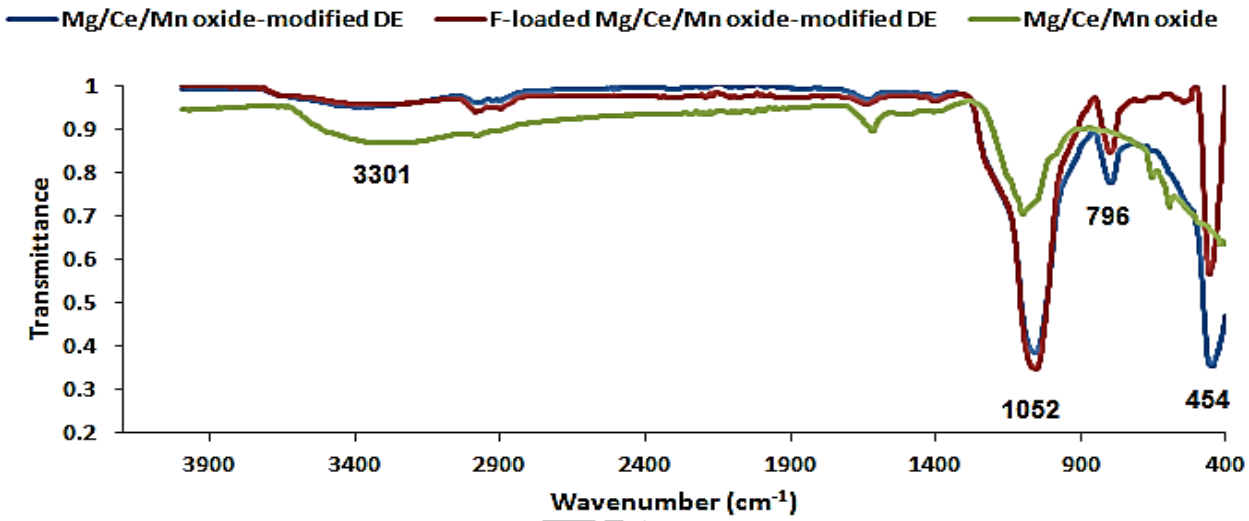

Figure 5 FTIR spectra of Mg/Ce/Mn oxide, Mg/Ce/Mn oxide-modified and F^- - loaded Mg/Ce/Mn oxide-modified DE.

3.3.6. pH at Point-of-zero-charge (pHpzc)

The change in pH ($p\Delta H = pH_e - pH_0$) was plotted against the initial pH (Figure 6). The pHpzc is the abscissa at the point where $p\Delta H = 0$. The pHpzc at the evaluated KCl concentrations was 5.45.

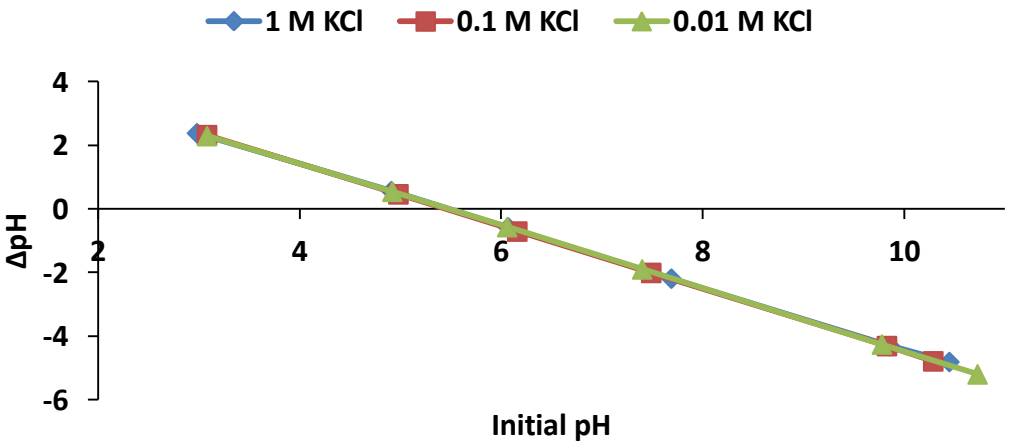

Figure 6 Determination of pH at point-of-zero charge of Mg/Ce/Mn oxide-modified DE for 1 M, 0.1 M and 0.01 M KCl (volume of solution: 25 mL, adsorbent dosage: 0.2 g, contact time: 24 h and shaking speed: 200 rpm).

3.4. Optimization of adsorption conditions

3.4.1. Contact time

The trends in the percent fluoride removal and the adsorption capacity at different contact times are shown in Figure 7. Within each evaluated sorbent dosage, there was no appreciable difference in the percent fluoride removal at the contact times. The fluoride sorption was so fast that with a sorbent dose of 0.1 g, the percent fluoride removal of 77.4% was attained within 2 min contact time. At the same sorbent dose, the highest fluoride removal of 80.0% was at 60 min equilibration time. A similar trend of fluoride removal within a short equilibration time was reported by Yao et al. (2009) and Izuagie et al. (2016, in press). The little step up of fluoride removal after 20 min to a near constant value is an indication that the sorbent was approaching its optimum performance as early as 20 min equilibration time.

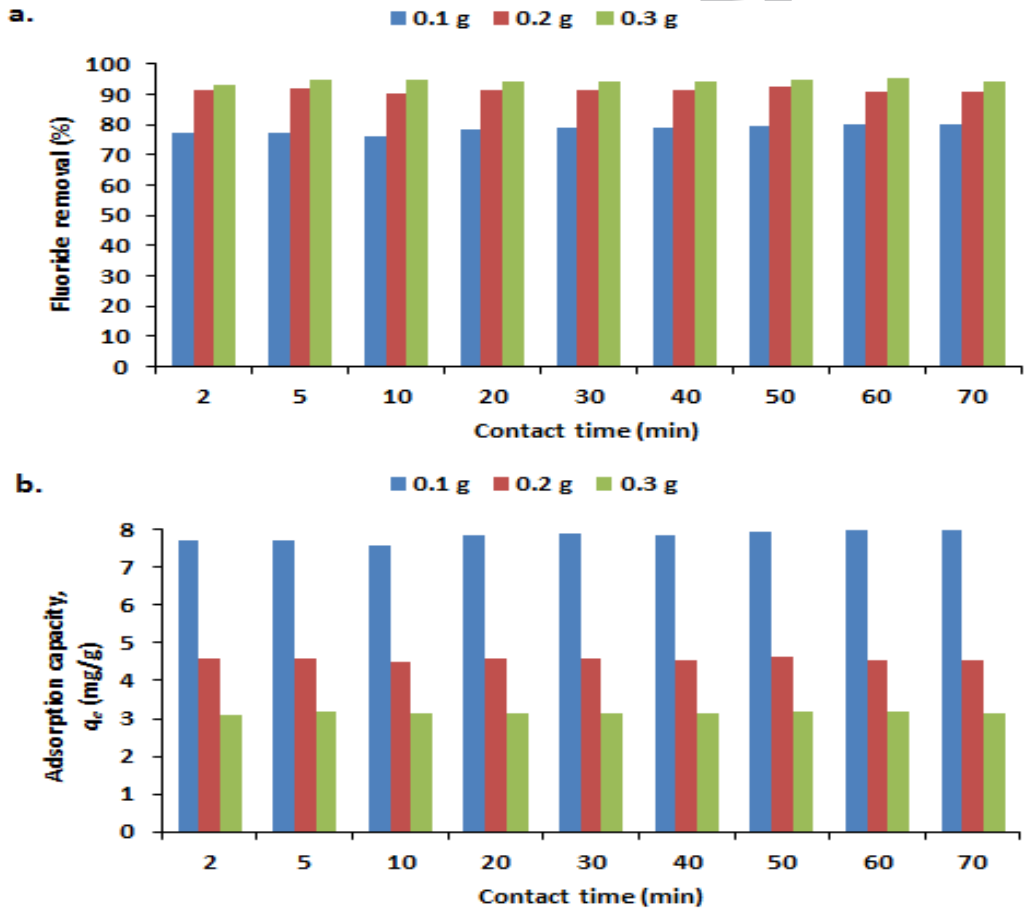

Figure 7 Variation of **a.** Percent fluoride removal and **b.** adsorption capacity with contact time at various adsorbent dosages (initial fluoride concentration: 10 mg/L, volume of solution: 100 mL, shaking speed: 200 rpm and temperature: 297 K).

3.4.2. Sorbent dosage

The results of the residual fluoride in the supernatants are presented in Figure 8. As the figure illustrates, there was a considerable rise in the percent fluoride removal with increase in the mass of sorbent from 0.1 g to 0.3 g (80.0% to 95.4%) after which the value increased moderately as the mass of sorbent increased. This finding is in agreement with reported cases of influence of sorbent dosage on fluoride removal (Jagtap et al., 2011; Manna et al., 2015). There was only a marginal increase in the percent fluoride removal above a dose of 0.3 g; the removal being 95.9 % and 98.0% for masses of 0.4 g and 1 g respectively, accounting for incremental difference of approximately 2%.

As sorbent dose was being increased from 0.1 g to 0.3 g, the number of active sites for fluoride sorption was increasing. Above 0.3 g, there was overlap of active sorption sites (Killedar and Bhatgava, 1990; Rai et al., 2004; Izuagie et al., 2015) to the effect that the net number of available active sorption sites was just a little higher than the one for 0.3 g. This explains why the values of percent fluoride removal at 0.3 g and 0.4 g are in particular very close (95.4 and 95.9% respectively). The adsorption capacity reduced expectedly as the sorbent dose increased.

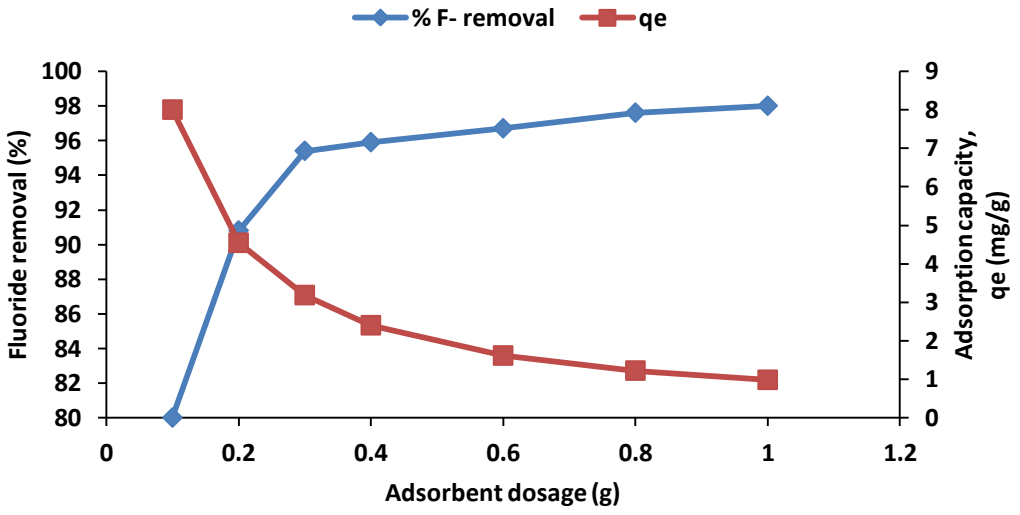

Figure 8 Percent fluoride removal and adsorption capacity as a function of adsorbent dosage (initial fluoride concentration: 10 mg/L, contact time: 60 min, shaking speed: 200 rpm and temperature: 297 K).

3.4.3. Initial fluoride concentration

The trend in the percent fluoride removal and adsorbent capacity with equilibrium fluoride concentration is reported in Figure 9. The amount of fluoride removed increased

slightly to a near constant value as the initial fluoride concentration increased from 10 to 30 mg/L. Beyond the latter; there was a gradual decrease in fluoride removal which became more apparent at the initial fluoride concentration of 50 mg/L. The percent fluoride removal was directly related to the initial concentration of fluoride within fluoride concentration range of 10-30 mg/L. Hence, fluoride concentration was the fluoride sorption rate driving force at the given concentration range. Above the initial concentration of 50 mg/L, there was a considerable decline in fluoride removal, a trend that has been widely reported (Wambu et al., 2011; Sakhare et al., 2012). The active sorption sites on the sorbent surface were nearing being saturated with adsorbed fluoride at high initial fluoride concentrations. The study showed a similar trend of fluoride removal at the three evaluated temperatures (Figure 9).

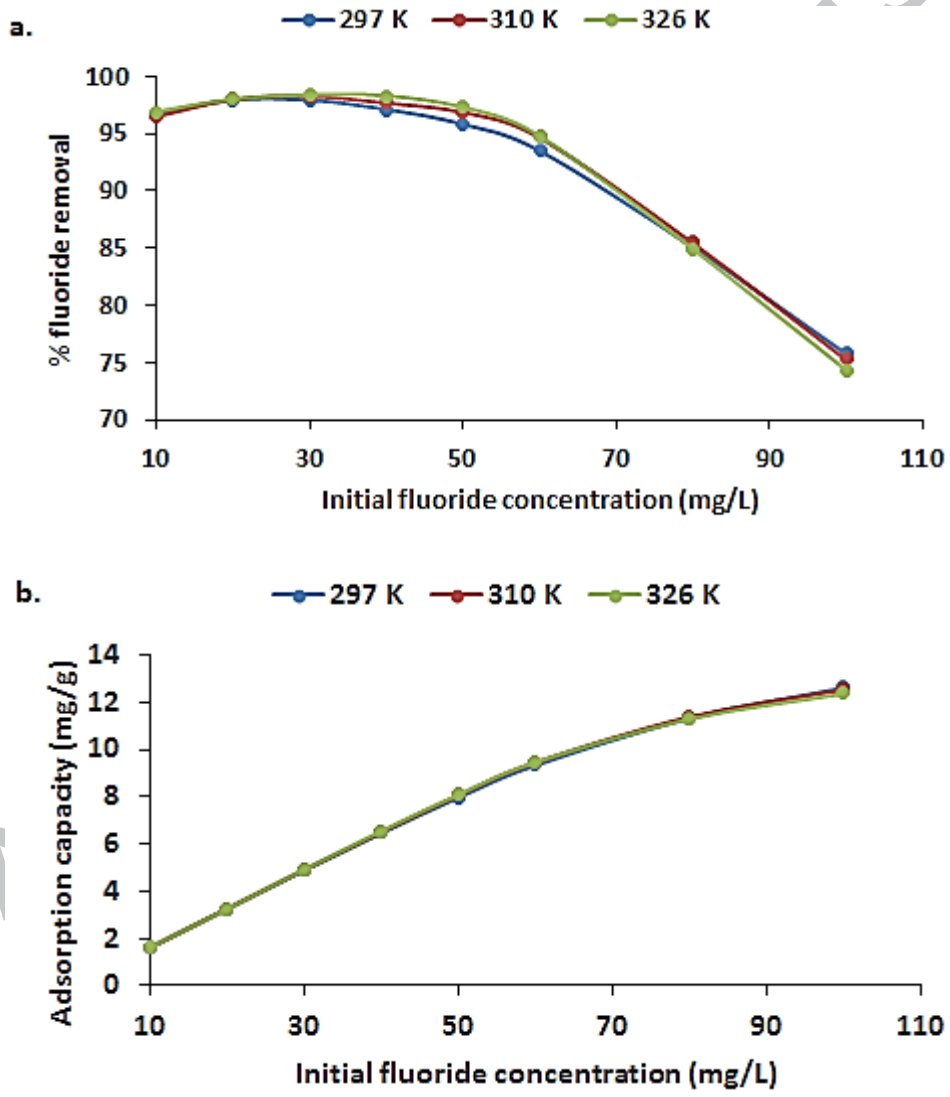

Figure 9 Variation of **a.** Percent fluoride removal and **b.** adsorption capacity with equilibrium fluoride concentration at different temperatures (contact time: 60 min, volume of solution: 100 mL, and shaking speed: 200 rpm).

The fluoride uptake capacity (adsorption capacity) of the sorbent increased almost linearly until the initial fluoride concentration of 60 mg/L where the trend of increase in adsorption capacity assumed another pattern showing that the sorbent surface was already nearing being completely filled. Similar trend in adsorption capacity with fluoride concentration has been reported in literature (Zhang et al., 2009; Matusik, 2014). The optimum adsorption capacities were obtained for solutions with the initial concentration of 100 mg/L at the three evaluated temperatures.

3.4.4. Solution pH

Fluoride removal by sorption is widely reported to be highly dependent on the pH of solution (Tripathy et al., 2006; Yadav et al., 2006; Kamble et al., 2009). Hence, defluoridation was carried out using 0.6 g/100 mL of sorbent and 9 mg/L fluoride solution at initial pH 2 to 12. The trend in the fluoride removal with respect to the evaluated pH is presented in Figure 10. Fluoride removal was highest and assumed a near constant value of 96.6% for solutions with initial pH range of ~ 4 to 9. This shows that the sorbent would exhibit its optimal defluoridation potential at the stated pH range. A slight decline in fluoride removal occurred for fluoride with initial pH 11. No noticeable fluoride removal occurred at pH 12.

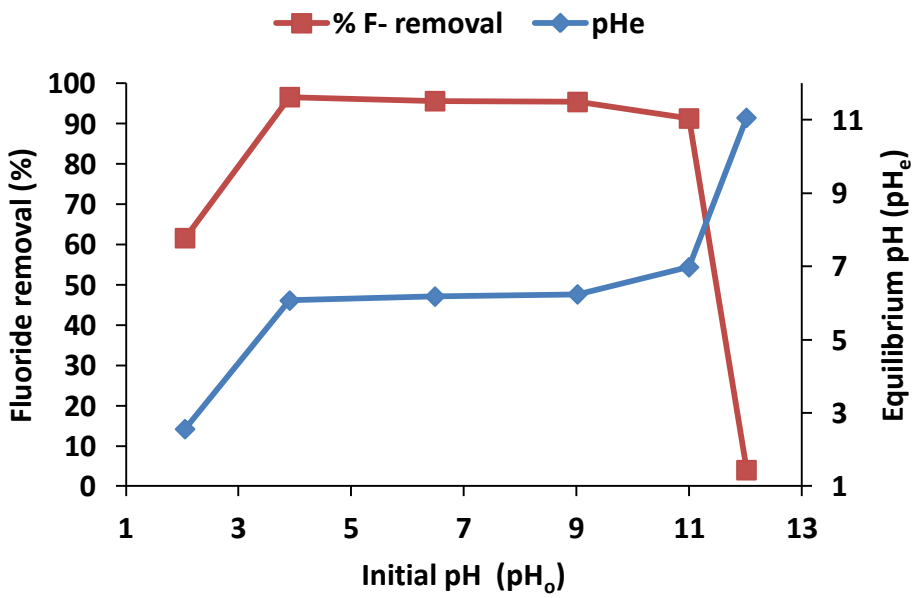

Figure 10 Fluoride removal as a function of initial solution pH (initial fluoride concentration: 9 mg/L, volume of solution: 100 mL, contact time: 60 min, shaking speed: 200 rpm and temperature: 297 K).

The behavior of the sorbent in fluoride removal at different pHs of solution can be explained on the basis of its pHpzc evaluated to be 5.45 (subsection 3.3.6). It therefore

follows that the surface of sorbent was negatively charged in solutions at which the equilibrium pH was greater than pHpzc. Fluoride removal would be ion-exchange in which the hydroxyl ions at the surface were being exchanged for the fluoride ions. In the sorbent composite, the dominant metal oxide/hydroxide responsible for fluoride removal is Ce oxide/hydroxide as established by Tables 1 and 2. Therefore, fluoride removal at pH > pHpzc was most probably as illustrated by Equation (3) to (5).

$$\blacksquare Ce(OH)_4^- + 3F^- \rightarrow \blacksquare Ce(OH)F_3^- + 3OH^- \quad (3)$$

$$\blacksquare Ce(OH)_4^- + 2F^- \rightarrow \blacksquare Ce(OH)_2F_2^- + 2OH^- \quad (4)$$

$$\blacksquare Ce(OH)_4^- + F^- \rightarrow \blacksquare Ce(OH)_3F^- + OH^- \quad (5)$$

For a neutral solution, pH = pHpzc fluoride would be removed by the sorbent in accordance with Equation (6):

$$\blacksquare Ce(OH)_3 + 3F^- \rightarrow \blacksquare CeF_3 + 3OH^- \quad (6)$$

The sorbent surface could assume a positive charge for a solution in which pH < pHpzc. This is illustrated by Equation (7):

$$\blacksquare Ce(OH)_3 + H^+ \rightarrow \blacksquare Ce(OH)_2^+ + H_2O \quad (7)$$

Fluoride removal at a positively charged surface would proceed as illustrated in Equation (8):

$$\blacksquare Ce(OH)_2^+ + 3F^- \rightarrow \blacksquare CeF_3 + 2OH^- \quad (8)$$

3.4.5. Temperature

As shown in Figure 11, the percent fluoride removal was approximately constant at each fluoride concentration for the evaluated temperatures. The same trend was observed for the adsorption capacity at different fluoride concentrations and temperatures (Figure 11b). Temperature change therefore had no effect on the extent of fluoride adsorbed.

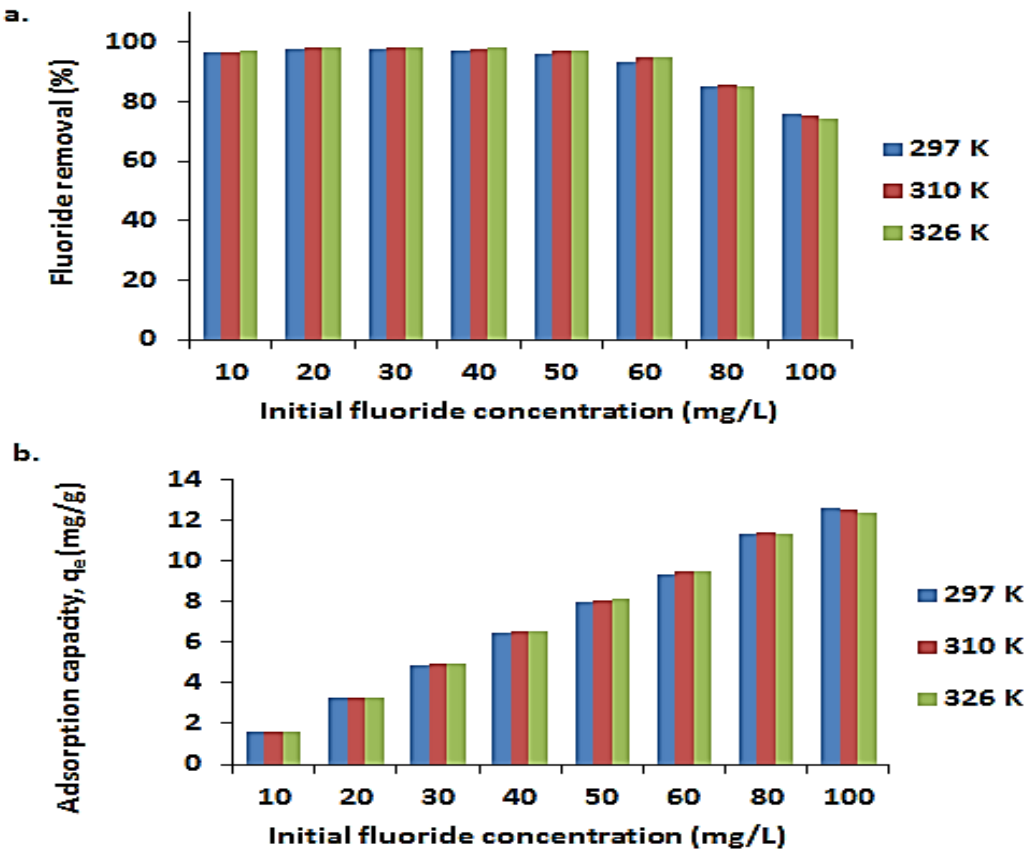

Figure 11 Variation of **a.** percent fluoride removal and **b.** adsorption capacity with temperatures (contact time: 60 min, volume of solution: 100 mL, and shaking speed: 200 rpm).

In Table 6, the defluoridation performances of Mg/Ce/Mn oxide-modified DE and some sorbents are compared. Considering the high fluoride removal at low contact time and small dosage to high fluoride solution concentration with the use of Mg/Ce/Mn oxide-modified DE sorbent compared to others, the former proves to be an effective sorbent for fluoride removal from fluoride contaminated water.

Table 6 Comparison of defluoridation performances of Mg/Ce/Mn oxide-modified DE and some sorbents

Adsorbent	Dosage (g/L)	Contact time (h)	Initial F^- concentration (mg/L)	% F^- removal	Treated water pH	Authors
Raw and calcined bauxite	12.5	1/2	8	93.8 (raw) 95.3 (calcined at 200 ^{0}C)	-	Sadiju et al., 2008.
Activated carbon	20	2	5	94	2	Tembhurkar and Dongre, 2006.
Acid-treated DE	500	1/6	1000	98.8 at 40 ^{0}C	3.32	Wambu et al., 2007.
Fe-Al-Ce trimetal oxide	0.150	24	84.5	68.4	7	Wu et al., 2007.
Neodymium – modified chitosan	2	24	20	98.2	7	Yao et al., 2009.
Cuttlefish	15	1	5	80	7.2	Nasr et al., 2011.
Mg/Ce/Mn oxide-modified DE	6	1	40	97.1	6.52	Present study.

3.5. Sorption isotherms

The pattern of fluoride sorption on the sorbent at equilibrium relative to the equilibrium concentration was studied using Langmuir and Freundlich isotherms. Langmuir isotherm differs from Freundlich isotherm in that it considers a monolayer adsorption of adsorbate onto homogeneous sorbent surface while the latter gives allowance for multisite adsorption onto a heterogeneous surface.

Langmuir isotherm is given as:

$$q_e = \frac{q_m K_L C_e}{1+K_L C_e} \quad (9)$$

where q_e is the adsorption capacity (mg/g), q_m is q_e for a complete monolayer (mg/g), C_e is the equilibrium concentration (mg/L) and K_L is the adsorption equilibrium constant (L/mg).

A linear form of Langmuir isotherm known as Langmuir-1 (Kinniburgh, 1986), given as:

$$\frac{C_e}{q_e} = \frac{1}{q_m} C_e + \frac{1}{K_L q_m} \quad (10)$$

was used for appraising the applicability of Langmuir isotherm to the sorption data.

The plot of $\frac{C_e}{q_e}$ values against C_e at the various temperatures assessed gave lines with high correlation coefficients implying a good fit of data to the Langmuir model as shown in Figure 12.

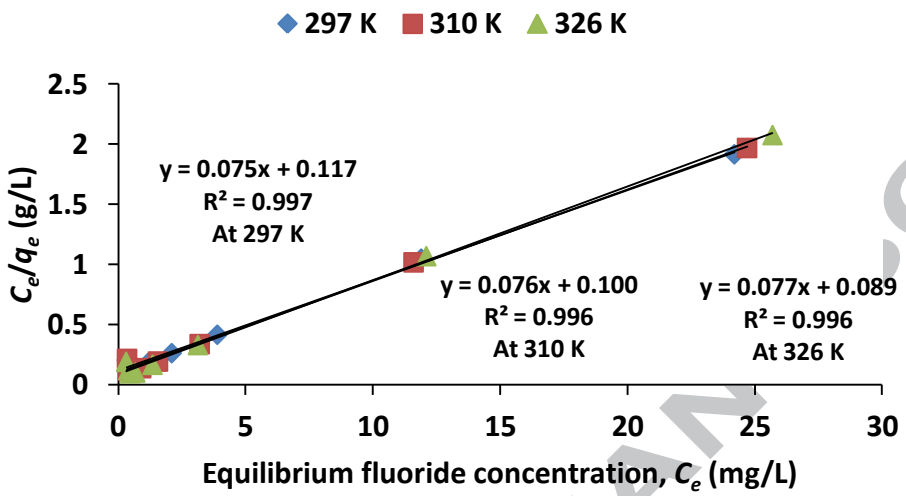

Figure 12 Langmuir isotherm plots at 297 K, 310 K and 326 K (contact time: 60 min, adsorbent dosage: 0.6 g, volume: 100 mL, shaking speed: 200 rpm).

The possibility of multisite adsorption of fluoride onto a rough sorbent surface was evaluated using the Freundlich isotherm given as:

$$q_e = K_F C_e^{1/n} \quad (11)$$

Introducing logarithm into Equation (11) gives the linear form:

$$\log q_e = \log K_F + \frac{1}{n} \log C_e \quad (12)$$

K_F and n are Freundlich constants whose values depend on experimental conditions. K_F represents the adsorption capacity while 1/n is the heterogeneity factor. Where 1/n values are much less than 1, the adsorbents are heterogeneous (Papageorgiou et al., 2006). The values of K_F and 1/n can be computed from the plots of $\log q_e$ against $\log C_e$.

The plot of $\log q_e$ against $\log C_e$ for the sorption data at 297 K, 310 K and 326 K gave points which deviated much from straight line especially at the lower fluoride concentrations (Figure 13). Comparatively, Langmuir isotherm gave a better fit for the sorption data than did Freundlich isotherm. Hence, there was rather a monolayer sorption of fluoride onto the sorption.

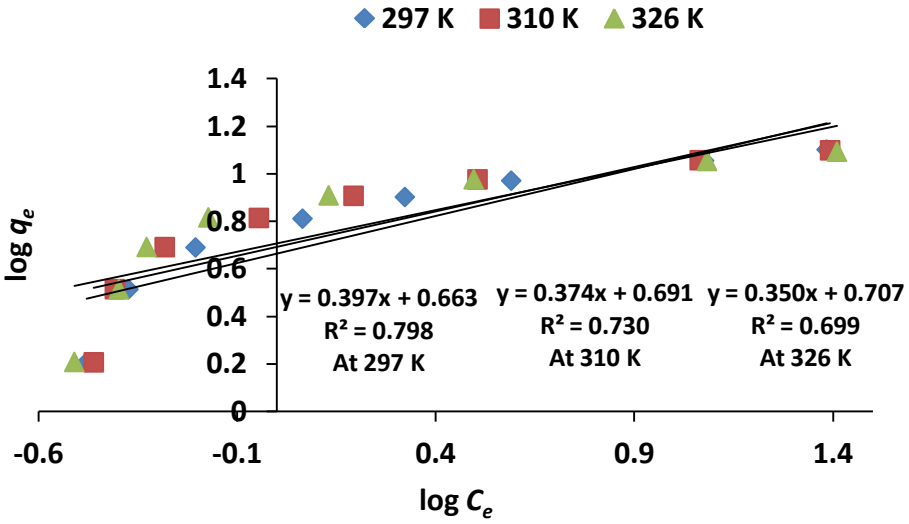

Figure 13 Freundlich isotherm plots at 297 K, 310 K and 326 K (contact time: 60 min, adsorbent dosage: 0.6 g, volume: 100 mL, shaking speed: 200 rpm).

The evaluated parameters of Langmuir and Freundlich isotherms at 297, 310 and 326 K are reported in Table 7.

Table 7 Calculated Langmuir and Freundlich isotherm parameters

	Langmuir isotherm constants				Freundlich isotherm constants		
Temperature (K)	q_m (mg/g)	K_L (L/mg)	K_L (m^3/kg)	R^2	*1/n*	K_F (mg/g)	R^2
297	13.333	0.6410	641.0	0.997	0.397	4.6026	0.798
310	13.158	0.7600	760.0	0.996	0.374	4.9091	0.730
326	12.987	0.8652	865.2	0.996	0.350	5.0933	0.699

The favorability of adsorption at the various concentrations of fluoride used for the Langmuir isotherm plots was estimated using the dimensionless separation factor, R_L, which is an essential feature of Langmuir model described by (Weber and Chakravorti, 1974).

The dimensionless separation factor is given as:

$$R_L = 1/(1 + K_L C_0) \quad (13)$$

K_L (L/mg) is the equilibrium constant obtained from Langmuir isotherm while C_0 (mg/L) is the initial adsorbate concentration.

R_L describes the shape of the isotherm to be unfavourable if $R_L > 1$, linear if $R_L = 1$ and favourable if $0 < R_L < 1$ (Weber and Chakravorti, 1974). The condition $0 < R_L < 1$ was fulfilled for all the initial concentrations considered at the evaluated temperatures (Figure 14). Hence, adsorption was favourable at those fluoride concentrations.

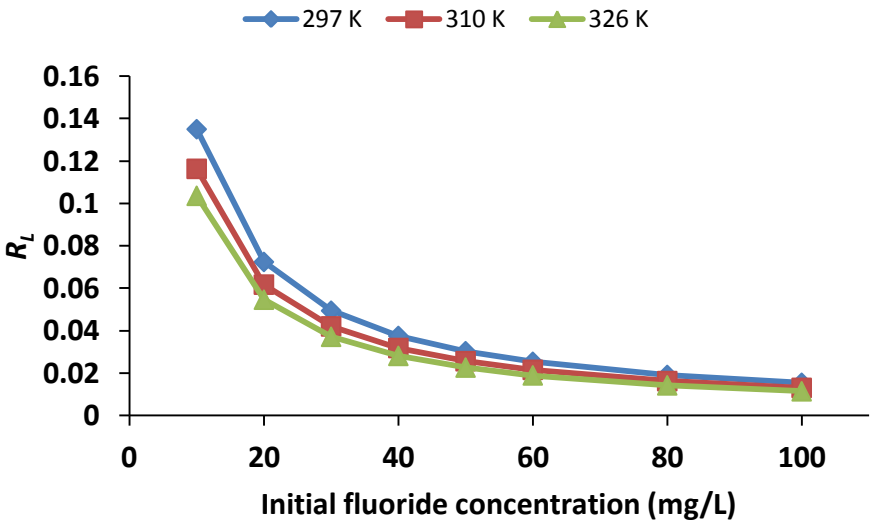

Figure 14 Values of dimensionless separation factor, R_L at different initial fluoride concentrations.

3.6. Adsorption thermodynamics

Temperature is one of the factors that greatly influence the spontaneity of a chemical process. However, the spontaneity of a chemical reaction is wholly determined by a thermodynamic quantity defined as the Gibbs free energy change, ΔG^0 (Jenkins, 2008). The Gibbs free energy is given as:

$$\Delta G^0 = \Delta H^0 - T\Delta S^0 \quad (14)$$

ΔH^0 is the standard enthalpy change while ΔS^0 is the standard entropy change.

For a spontaneous sorption process, ΔG^0 must have a negative value.

In sorption equilibria, the equilibrium constant, K_L which is the Langmuir's constant is related to the Gibbs free energy change by the equation:

$$\Delta G^0 = -RT \ln K_L \quad (15)$$

ΔG^0 is the standard Gibbs free energy change and R is the molar gas constant, 8.314 J mol^{-1} K^{-1}.

$$\ln K_L = -\frac{\Delta H^0}{RT} + \frac{\Delta S^0}{R} \quad (16)$$

ΔH^0 is known as the standard enthalpy change.

The linear form

$$\ln K_L = -\frac{\Delta H^0}{RT} + \text{constant} \quad (17)$$

is suitable for graphical determination of the standard enthalpy change from the slope of the linear plot of $\ln K_L$ against $1/T$.

The Gibbs free energy change calculated for the sorption data at the evaluated temperatures have negative values as shown in Table 8.

Plotting ln K_L against 1/T gave a straight line (Figure 15) from which ΔH^0 was calculated to be 8281.58 J/mol.

Table 8 Adsorption thermodynamic parameters

T (K)	1/T (1/K)	ln K_L	K_L (m^3/kg)	ΔG^0 (J/mol)
297	0.003367	6.463	641	−15,958.89
310	0.003226	6.633	760	−17,096.32
326	0.003067	6.763	865	−18,330.09

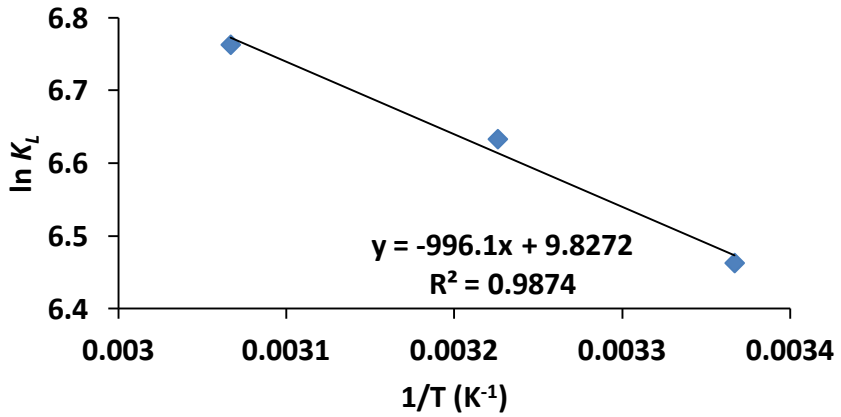

Figure 15 ln K_L as a function of reciprocal of adsorption temperatures.

3.7. Adsorption kinetics

The Lagergren pseudo-first-order (Lagergren, 1898) and the pseudo-second-order models which are reaction-based models were used to evaluate the kinetic order of the sorption process.

The pseudo-first-order is given as:

$$\frac{dq_t}{dt} = k_1(q_e - q_t) \quad (18)$$

q_t (mg/g) is the fluoride concentration at any time t, q_e(mg/g) is the maximum sorption capacity of the pseudo-first-order and k_1(min^{-1}) is the pseudo-first-order rate constant.

On integration, Equation (18) gives the linear equation:

$$\log\,(q_e - q_t) = -\frac{k_1}{2.303}\,t + \log q_e \quad (19)$$

The rate constant, k_1 and the calculated maximum adsorption capacity, q_e are obtained from the linear plot of log (q_e - q_t) against time, t.

The pseudo-first-order plot was a scatter; hence, the model was not an applicable kinetic model to the sorption data.

The pseudo-second-order kinetic model for adsorption is given as:

$$\frac{dq_t}{dt} = k_2(q_e - q_t)^2 \quad (20)$$

q_t (mg/g) is the fluoride concentration at any time *t*, q_e (mg/g) is the maximum sorption capacity of the pseudo-second-order and k_2 (g/ (mg min)) is the rate constant for the pseudo-second-order process.

On integration, Equation (20) gives the linear form of the pseudo-second-order:

$$\frac{t}{q_t} = \frac{1}{k_2\, q_e^2} + \frac{t}{q_e} \quad (21)$$

The plot of t/q_t values against time *t* for the experiments with adsorbent dosages of 0.1, 0.2 and 0.3 g gave lines with very high correlation coefficients (Figure 16). The good fit of data to the model is an indication that the pseudo-second-order model was the appropriate kinetic model to describe the sorption kinetics. It is also implied that fluoride sorption was chemisorption. That fluoride sorption obeyed only the pseudo-second-order model was further established by comparing the values of the calculated q_e and the experimental q_e as presented in Table 9.

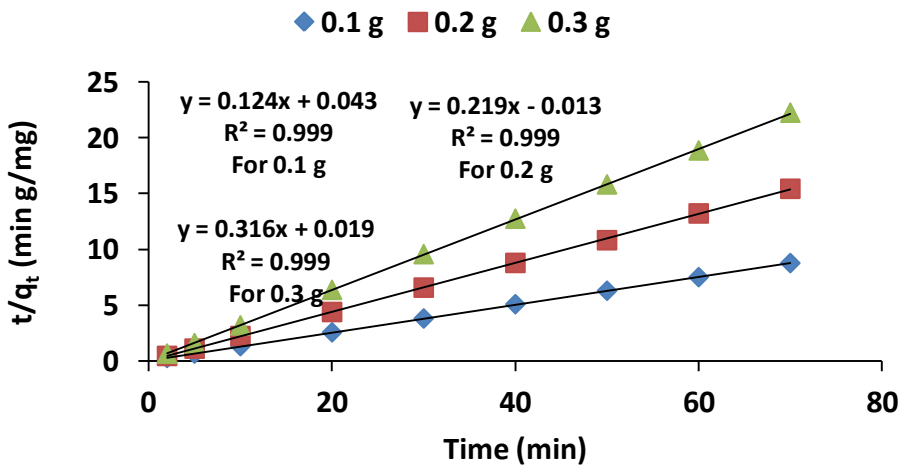

Figure 16 Pseudo-second-order plots for 0.1, 0.2 and 0.3 g sorbent (initial fluoride concentration: 10 mg/L, volume of solution: 100 mL, shaking speed: 200 rpm and temperature: 297 K).

Table 9 Pseudo-second-order parameters at different adsorbent dosages

Adsorbent dosage (g)	Equation	Experimental q_2 (mg/g)	Calculated q_2 (mg/g)
0.1	y = 0.124x + 0.043	8.0000	8.0645
0.2	y = 0.219x - 0.013	4.6245	4.5662
0.3	y = 0.316x + 0.019	3.1810	3.1646

3.7.1. Intra-particle and external diffusions

The migration of adsorbate through the pores of adsorbent could be an adsorption rate limiting step if on the account of the adsorbent size there is some strain for the adsorbate migrating through the adsorbent surface. The model evolved by Weber and Morris (1963) was used to appraise the likelihood of intra-particle diffusion being the sorption rate controlling mechanism of fluoride sorption.

The model given as:

$$q_t = k_{id}\sqrt{t} + I \quad (22)$$

k_{id} is the intra-particle diffusion rate constant (mg/(g $min^{1/2}$)) and *I* (mg/g) is a constant that has to do with the thickness of the boundary layer. A linear plot of q_t against $\sqrt{t}$ is an indication of intra-particle diffusion being the sorption rate controlling step. However, the scatter plot obtained indicated that intra-particle diffusion was not the rate-controlling factor. This looks justifiable considering the ratio of ionic diameter of fluoride (2.66 Å) (Ruben, 1985) to that of the least pore size of the sorbent (20.12 Å) determined by BET (Figure 3). Fluoride ion would diffuse through the sorbent without inhibition.

The possibility of external diffusion of sorbent being the sorption rate controlling step was evaluated using the model by Lee et al. (1999).

The diffusion model is given as:

$$\ln\frac{C_t}{C_0} = -k_f\frac{A}{V}t \quad (23)$$

C_0 (mg/L) is the initial fluoride concentration, C_t (mg/L) is the fluoride concentration at time *t*, *A/V* is the external adsorption area to the total solution volume, *t* is the adsorption time, and $k_f$is the external diffusion coefficient. A linear plot of $\ln\frac{C_t}{C_0}$ against *t* is an indication of external diffusion being the sorption rate controlling process. Modelling the data using Equation (23) resulted in bilinear plots. The trend in the profile was the same even at

different experimental temperatures as presented in Figure 17. The first linear portion was from 2 - 20 min contact time, while the second linear portion was from 30 to 70 min contact time. The bilinear plots indicate a two-mode influence of external diffusion on the sorption rate. External diffusion is therefore the rate limiting step for the fluoride sorption.

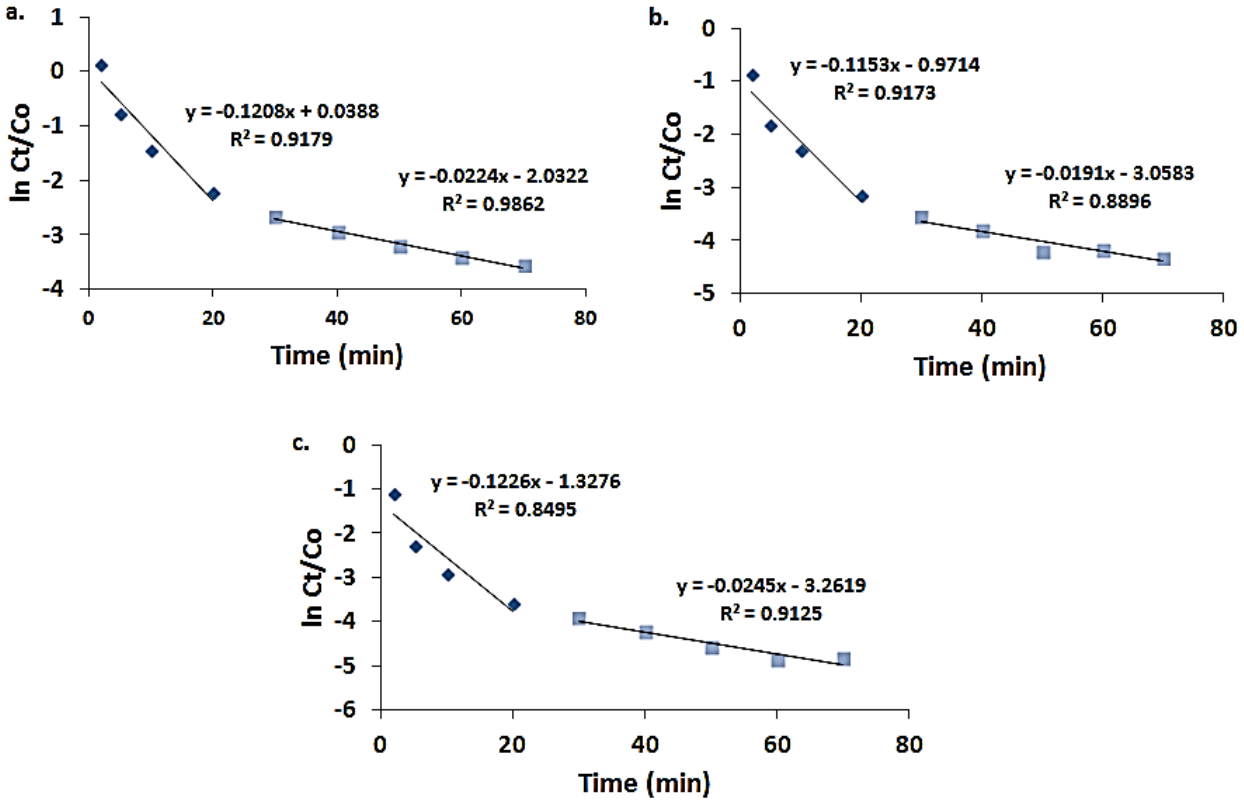

Figure 17 External diffusion plots for 0.1 g, 0.2 g and 0.3 g sorbent dosages (initial fluoride concentration: 10 mg/L, volume of solution: 100 mL, shaking speed: 200 rpm and temperature: 297 K).

3.8. Effect of co-existing anions

The results of the fluoride analysis of supernatants from defluoridated anion-spiked water presented in Figure 18 give the extent to which the presence of each anion could possibly enhance or inhibit fluoride removal. The result reported for blank indicated competing anion-free water. As Figure 18 reveals, the percent fluoride removal varied with the type of anion. The presence of Cl^-, NO_3^- and SO_4^{2-} in solution was observed to enhance fluoride removal as the amount of fluoride removed increased slightly. CO_3^{2-} appeared to be competing with fluoride in solution as it lowered the amount of fluoride removal slightly from 96.7% to 95.3%. The presence of PO_4^{3-} in solution had no effect on fluoride removal. The equilibrium pH ranged between 6.17 and 6.28.

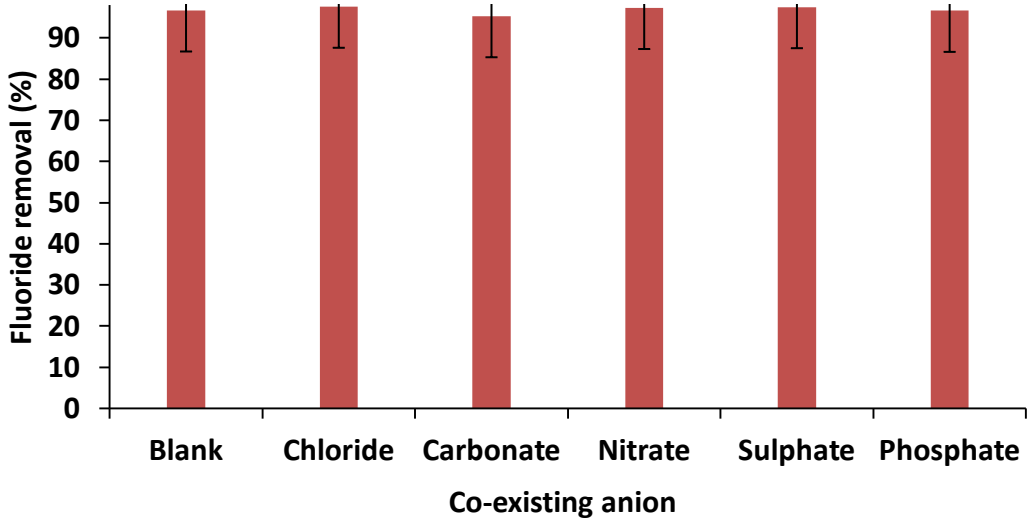

Figure 18 Percent fluoride removal in the presence of co-existing anions (initial fluoride concentration: 10 mg/L, initial anion concentration: 5 mg/L, volume of solution: 100 mL, contact time: 60 min, shaking speed: 200 rpm and temperature: 297 K).

3.9. Sorbent regeneration and reuse

Figure 19 shows the trend in the percent fluoride removal from treated water at various cycles of defluoridation. The fluoride removal potential of the regenerated sorbent reduced with use. Fluoride removal by sorbent regenerated with NaOH was observed to be very low when compared to that regenerated with K_2SO_4. With the use of NaOH as regenerant, the amount of sorbent lost as a result of silica dissolution in alkaline medium was appreciably high. With loss of sorbent no appreciable fluoride removal was observed from the first to the fourth defluoridation cycle. The reagent is therefore inappropriate for regeneration of amorphous silica based sorbent such as Mg/Ce/Mn oxide-modified DE.

The use of 0.1 M K_2SO_4 solution presented a slightly acidic medium for the spent sorbent regeneration. The results of percent fluoride removal at the first, second and third cycles were 60.8%, 40.6% and 35.0% respectively. At the second cycle of defluoridation of 10 mg/L fluoride solution using a sorbent dosage of 0.8 g/100 mL, fluoride concentration would be reduced to 3.92 mg/L. This value is much higher than the WHO permissible limit of 1.5 mg/L fluoride in drinking water (WHO, 2011). Regeneration of spent Mg/Ce/Mn oxide-modified DE is therefore not encouraged for groundwater with high fluoride content.

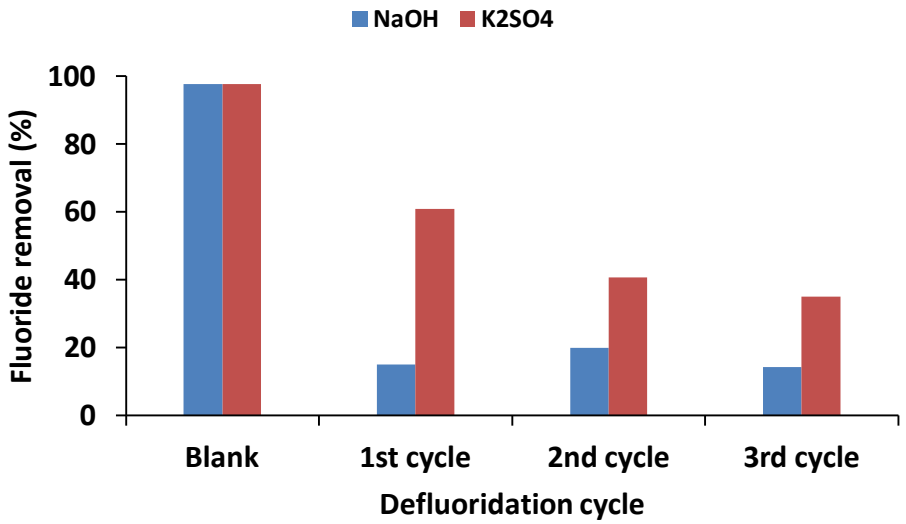

Figure 19 Percent fluoride removal as a function of defluoridation cycle using 0.01 M NaOH and 0.1 M K_2SO_4 as regenerants (initial fluoride concentration: 10 mg/L, volume of solution: 100 mL, adsorbent dosage: 0.8 g contact time: 60 min, temperature: 297 K and shaking speed: 200 rpm).

4. Conclusions

SEM images, EDX, major and trace elements analyses of raw DE and synthesized Mg/Ce/Mn oxide-modified DE (sorbent) provided evidence that there was a deposit of metal oxides on raw DE after metal oxide modification.

Fluoride uptake from solution occurred above the pHpzc of 5.45, establishing exchange of hydroxyl groups on surface of sorbent with fluoride ions in solution.

The highest adsorption capacity of sorbent was 12.633 mg/g, at the initial fluoride concentration of 100 mg/L at 297 K. Sorbent was so efficient such that fluoride removal was 97.1% at solid/liquid ratio of 0.6 g/100 mL (initial fluoride concentration: 40 mg/L, contact time: 60 min, temperature: 297 K, and shaking speed: 200 rpm). It was observed that temperature change had no appreciable effect on fluoride removal.

CO_3^{2-} was observed to cause a slight reduction of F^- removal, Cl^-, NO_3^- and SO_4^{2-} gave a small increase in F^- removal while the presence of PO_4^{3-} in solution had no effect on F^- removal.

Sorption data conformed better to Langmuir isotherm than Freundlich isotherm while pseudo-second-order model was a more suitable model than pseudo-first-order model. Hence, fluoride uptake was by chemisorption.

External diffusion plots showed that it was likely to be the rate limiting step for F^- sorption onto the adsorbent surface.

K_2SO_4 solution proved to be a better regenerant for spent sorbent compared to NaOH and Na_2CO_3.

Acknowledgements

This work was supported by WRC Project No. K5/2363/3, NRF Project No. CSUR13092849176, Grant No. 90288, THRIP Project No. TP12082610644 and Directorate of Research & Innovation, University of Venda and TETFund Grant, Nigeria.

References

Abdulrahmani, A., 1996. Fluoride content in drinking water supplies of Riyadh, Saudi Arabia, Environ Monit. Assess. 48, 261–272.

Altman, P.L. and Dittmer, D.S., 1961. Blood and other Body Fluids/Analysis and Compilation. Federation of American Societies for Experimental Biology (Biological Handbooks), Washington, DC.

Amor, Z., Taky, M., Malki, S., Nicolas, S., Elmidaoui, A., 2001. Fluoride removal from brackish water by electrodialysis. Desalination, 133, 215–223.

Antonides, L.E., 1998. Diatomite. US Geological Survey Mineral Commodity Summaries. United States of America.

Chen, N., Zhang, Z., Feng, C., Zhu, D., Yang, Y., Sugiura, N., 2011. Preparation and characterization of porous granular ceramic containing dispersed aluminium and iron oxides as adsorbents for fluoride removal from aqueous solution. J. Hazard. Mater. 186, 863–868.

Datsko, T.Ya., Zelentsov, V.I., Dvornikova, E.E., 2011. Physicochemical and adsorption_structural properties of diatomite modified with aluminum compounds. Surface Eng. Appl. Electrochem. 47 (6), 530–539.

Daw, R.K., 2004. Experiences with domestic defluoridation in India. 30th WEDC International Conference, Vientiane, Lao PDR, 467-473.

Gambhir, R.S., Kapoor, V., Nirola, A., Sohi, R., Bansal, V., 2012. Water pollution: impact of pollutants and new promising techniques in purification process. J. Hum. Ecol., 37 (2), 103-109.

Hichour, M., Persin, F., Sandeaux, J., Gavach, C., 2000. Fluoride removal from waters by Donnan dialysis, Sep. Purif. Technol. 18, 1–11.

Izuagie A.A., Gitari W.M., Gumbo J.R., 2015. Defluoridation of groundwater using diatomaceous earth: optimization of adsorption conditions, kinetics and leached metals risk assessment. Desalin. Water Treat. 1-13. DOI: 10.1080/19443994.2015.1083894.

Izuagie, A.A., Gitari, W.M., Gumbo, J.R., 2016. Synthesis and performance evaluation of Al/Fe oxide coated diatomaceous earth in groundwater defluoridation: towards fluorosis mitigation. J. Environ. Sci. Health A: Tox. Hazard. Subst. Environ. Eng. 1-16. DOI:

10.1080/10934529.2016.1181445.

Jagtap, S., Yenkie, M.K.N., Labhsetwar, N., Rayalu, S., 2011. Defluoridation of drinking water using chitosan based mesoporous alumina. Micropor. Mesopor. Mat. 142, 454–463.

Jenkins, G.N., 1978. The Physiology and Biochemistry of the Mouth, fourth ed. Blackwell Scientific Publication, London.

Jenkins, H.D.B., 2008. Chemical Thermodynamics at a Glance. Blackwell Publishing Ltd.: Oxford.

Kamble, S.P., Dixit, P., Rayalu, S.S., Labhsetwar, N.K., 2009. Defluoridation of drinking water using chemically modified bentonite clay. Desalination. 249, 687–693.

Khraisheh, M.A.M.; Al-Degs, Y.S.; Mcminn, W.A.M., 2004a. Remediation of wastewater containing heavy metals using raw and modified diatomite. Chem. Eng. J. 99, 177–184.

Khraisheh, M.A.M.; Al-Ghouti, M.A.; Allen, S.J.; Ahmad, M.N.M., 2004b. The effect of pH, temperature and molecular size on the removal of dyes from textile effluent using manganese oxides modified diatomite. Water Environ. Res. 76, 2655-2663.

Killedar, D.J., Bhatgava, D.S., 1990. Feasibility of fluoride adsorption on bone charcoal. J. Inst. Eng. 70, 47–49.

Kinniburgh, D.G., 1986. General purpose adsorption isotherms. Environ. Sci. Technol. 20 (9), 895-904.

Lagergren, S. 1898. Zur theorie der sogenannten adsorption gelöster stoffe (About the theory of so-called adsorption of soluble substances). K. Sven. Vetensk. Akad. Handl., 24 (4), 1-39.

Lee, C.K., Low, K.S., 1999. Chew, S.L. Removal of anion dyes by water hyacinth roots. Adv. Environ. Res. 3, 343-351.

Lemonas, J.F., 1997. Diatomite. American Ceramic Society Bulletin, 76, 92-95.

Manna, S., Saha, P., Roy, D., Sen, R., Adhikari, B., 2015. Defluoridation potential of jute fibers grafted with fatty acyl chain. Appl. Surf. Sci. 356, 30–38.

Matusik, J., 2014. Arsenate, orthophosphate, sulfate, and nitrate sorption equilibria and kinetics for halloysite and kaolinites with an induced positive charge. Chem. Eng. J. 246, 244–253.

Mjengera, H., Mkongo, G. 2003. Appropriate defluoridation technology for use in fluorotic areas in Tanzania, Phys. Chem. Earth. 28, 1097–1104.

Nasr, A.B., Walha, K., Charcosset, C., Amar, R.B., 2011. Removal of fluoride ions using cuttlefish bones. J. Fluorine Chem. 132, 57-62.
Ncube, E.J., Schutte, C.F., 2005. The occurrence of fluoride in South African groundwater: A water quality and health problem. Water SA. 31 (1), 35-40.

Obi, C.L., Potgieter, N., Bessong, P.O., Matsaung, G., 2002. Assessment of the microbial quality of river water sources in rural Venda communities in South Africa. Water SA. 28 (3), 287-292.

Oladoja, N.A., Helmreich, B., 2014. Batch defluoridation appraisal of aluminium oxide infused diatomaceous earth. Chem. Eng. J. 258, 51–61.

Papageorgiou, K.S.; Katsaros, K.F.; Kouvelos, P.E.; Nolan, W.J.; LeDeit, H.; Kanellopoulos, K.N., 2006. Heavy metal sorption by calcium alginate beads from *Laminaria digitata*. J. Hazard. Mater. 137, 1765–1772.

Rai, M., Pathan, M., Khan, A., Farooqui, M., Zaheer, A., 2004. A study of the removal of dyes by Goda sand. J. Indian Chem. Soc. 81, 484–487.

Ruben, S., 1985. Handbook of the Elements. Open Court Publishing Company, La Salle, Illinois, USA.

Sadiju, S.M.I., Masamba, W.R.L., Thole, B., Mwatseteza, J.F., 2008. Groundwater fluoride levels in villages of Southern Malawi and removal studies using bauxite. Inter. J. Phys. Sci. 3 (1), 1-11.

Sakhare N., Lunge, S., Rayalu, S., Bakardjiva, S., Subrt, J., Devotta, S., and Labhsetwar, N., 2012. Defluoridation of water using calcium aluminate material. Chem. Eng. J. 203, 406–414.

Tembhurkar, A.R., Dongre, S., 2006. Studies on fluoride removal using adsorption process. J. Environ. Sci. Eng. 48 (3), 151-156.

Teri, E.M., 1982. Endemic Fluorosis: Some Clinical and Epidemiological Aspects of Fluorosis with Specific Reference to Maji ya Chai Area, Arusha Region. A report on domestic water health standards with emphasis on fluoride, Ministry of Water and Energy, Arusha, Tanzania.

Tripathy, S.S., Bersillon, J-L., Gopal, K., 2006. Removal of fluoride from drinking water by adsorption onto alum-impregnated activated alumina. Sep. Purif. Technol. 50, 310–317.

Upadhyay, S.K., 2006. Chemical Kinetics and Reaction Dynamics. Springer and Anamaya Publishers, New York and New Delhi

Wambu, E.W., Onindo, C.O., Ambusso, W.J. & Muthaka, G.K., 2011. Fluoride adsorption onto acid-treated diatomaceous mineral from Kenya. Mater. Sci. Appl. 2, 1654-1660.

Wang, J., Kang, D., Yu, X., Ge, M. and Chen, Y., 2015. Synthesis and characterization of Mg–Fe–La trimetal composite as an adsorbent for fluoride removal. Chem. Eng. J. 264, 506–513.

Weber, T.W., Chakravorti, R.K., 1974. Pore and solid diffusion models for fixed bed adsorbents. AIChE J. 20, 228-238.

Weber, W.J.; Morris, J.C., 1963. Kinetics of adsorption on carbon from solution. J. Sanit. Eng. Div. /Am. Soc. Civ. Eng. 89, 31-60.

World Health Organization (WHO), 2011. Chemical fact sheets. Guidelines for Drinking-water Quality, fourth ed. Gutenberg, Malta.

Wu, X., Zhang, Y., Dou, X. & Yang, M., 2007. Fluoride removal performance of a novel Fe-Al-Ce trimetal oxide adsorbent. Chemosphere, 69, 1758-1764.

Xiong, W., Peng, J., 2008. Development and characterization of ferrihydrite-modified diatomite as a phosphorus adsorbent. Water Res. 42, 4869-4877.

Yadav, A.K., Kaushik, C.P., Haritash, A.K., Kansal, A., Rani, N., 2006. Defluoridation of groundwater using brick powder as an adsorbent. J. Hazard. Mater. 128, 289–293.

Yao, R., Meng, F., Zhang, L., Ma, D., Wang, M., 2009. Defluoridation of water using neodymium-modified chitosan. J. Hazard. Mater. 165, 454-460.

Zhang, J., Xie, S., Ho, Y-S., 2009. Removal of fluoride ions from aqueous solution using modified attapulgite as adsorbent. J. Hazard. Mater. 165, 218–222.